PROPOSAL TO PAC30

Hard Exclusive Electroproduction of π^0 and η with CLAS12

K. Joo[†], M. Ungaro[†]

University of Connecticut, Storrs, Connecticut 06269, USA

H. Avakian, V. Burkert, L. Elouadrhiri, C. Weiss[†]

Jefferson Lab, Newport News, VA 23606, USA

H. Egiyan, M. Holtrop

University of New Hampshire, Durham, New Hampshire 03824-3568

V. Kubarovsky[†], P. Stoler[†,*]

Department of Physics, Rensselaer Polytechnic Institute, Troy, NY 12181, USA

J. Ball, R. De Masi, M. Garçon, F.-X. Girod, M. Guidal,
M. Mac Cormick, M. Mazouz, B. Michel, S. Niccolai, B. Pire,
S. Procureur, F. Sabatié, E. Voutier, S. Wallon

LPC (Clermont) / LPSC (Grenoble) / IPNO & LPT (Orsay) CPhT-Polytechnique (Palaiseau)
SPhN (Saclay) / CEA/DSM/DAPNIA & CNRS/IN2P3, France

I. Bedlinsky, S. Kuleshov, O. Pogorelko, N. Pivnyuk, A. Vlassov

Institute for Theoretical and Experimental Physics, Moscow 117218, Russia

and the CLAS Collaboration

[†] Co-spokesperson

* Contact: stoler@rpi.edu

Technical participation of research groups

Rensselaer Polytechnic Institute

The RPI group is actively involved in this proposal using CLAS12 base equipment.
Paul Stoler is a member of the CLAS12 Steering Committee. Among the CLAS12 baseline equipment, our group is involved in the design, prototyping, construction and testing of the high threshold Cerenkov counter (HTCC) and modification of the low threshold Cerenkov counter (LTCC). Currently, Paul Stoler is serving as a coordinator HTCD and LTCD group involved in the effort. Valery Kubarovsky is designing and building the apparatus for testing the prototype components. Two undergraduates Jason Sanchez and Stephanie Tomasulo, are spending the summer at JLab working respectively on prototype mirror fabrication and computer aided optics design and simulation. The group will continue to be fully involved as needed. The group is currently funded by NSF and RPI. Additional sources of funding will be sought as appropriate.

University of Connecticut

The University of Connecticut (UConn) group is actively involved in this proposal using CLAS12 baseline equipment.

Among the CLAS12 baseline equipment, our group is sharing the responsibility for the design, prototyping, construction and testing of the high threshold Cerenkov counter (HTCC). One faculty member (Kyungseon Joo), one post-doc (Maurizio Ungaro), four graduate students (Bo Zhao, Nikolay Markov, Taisia Mineeva and Igor Konyukov) are already, or will be, working on this project.

The University of Connecticut Research Foundation (UCRF) already funded $32,000 for the equipment purchase for the HTCC prototyping project. UConn is also providing a clean room facility for this project and providing funding for a half postdoctoral support and a half graduate student support for the next two years for our group's JLab research activities. The group is currently funded by the U.S Department of Energy (DOE). Additional sources of funding will be sought as appropriate.

Beyond the baseline equipment, the group is also deeply involved in software planning and development for CLAS12. The group was recently awarded a DOE SBIR/STTR Phase

I grant with a software company, CyberConnect EZ to develop a software framework to archive a large scale nuclear physics experiment data base.

DAPNIA/SPhN-Saclay, France

The DAPNIA/SPhN-Saclay group is actively involved in this proposal, as well as in one other proposal using CLAS12, and one other proposal for Hall A.

Among CLAS12 baseline equipment, the group intends to take responsibility for the design, prototyping, construction and testing of the central tracker (both the cylindrical part and the forward part). The group has started working on an option based on cylindrical Micromegas detectors. Provided this is shown to work as designed, the group anticipates that this option will be examined in comparison with the Silicon Strip tracker, toward the end of 2007 or the beginning of 2008. Four research staff members and four technicians/engineers are likely to work at least part time on this project in the next few years. Funding for the group is from CEA-France. Additional sources of funding (ANR-France, European Union 7th PCRD) will be sought as appropriate.

In case the Micromegas option is not suitable, or not selected for valid reasons, the group would study other technical participations in the CLAS12 baseline equipment.

Beyond the baseline equipment, the group is also interested in exploring neutral particle detection (mostly neutrons) in the central detector of CLAS12, in the so far empty space between TOF scintillators and solenoid cryostat.

University of New Hampshire

The University of New Hampshire Nuclear Physics group is actively involved in this proposal, as well as three other proposal using CLAS12.

The UNH group is committed to significant contributions in the development of the CLAS12 software. Maurik Holtrop is currently chair of the CLAS12 GEANT4 simulation group to which our post-doc Hovanes Egiyan is also contributing. Since currently the main software efforts for CLAS12 are in the area of simulation we are also part of and contributing to the general CLAS12 Software group. Current manpower commitments to this effort are 0.15 FTE of a faculty and 0.4 FTE of one post-doc. We expect to increase this effort as our CLAS activities wind down and our CLAS12 activities pick up and we expect to attract

some talented undergraduate students to this project.

Among CLAS12 baseline equipment, the group intends to take responsibility for the design, prototyping, construction and testing of the silicon vertex detector and perhaps the inner detector's silicon tracking detectors. Faculty member Maurik Holtrop is likely to work at least part time on this project in the next few years and is likely to be joined by Jim Connel, a cosmic ray experimentalist with a background in nuclear physics, who is very interested in joining the vertex detector project. He has considerable experience with silicon detectors for space observations. Funding for the group is from DOE and additional sources of funding will be sought for this project to bring aboard Prof. Connel. If funded we are likely to attract a post-doc, a graduate student and one or two undergraduate students to this project.

Beyond the baseline equipment, the group is also interested in exploring an extended inner calorimeter for CLAS12.

Institute for Theoretical and Experimental Physics

The ITEP group is actively involved in this proposal and in the CLAS12 upgrade. The ITEP team is responsible for the design, prototyping, construction and testing of the superconducting magnets (TORUS and Solenoid), the tracking system, and the high threshold Cerenkov counter (HTCC). Oleg Pogorelko is serving as a coordinator for the magnet design. Alex Vlassov is doing the Monte Carlo program for the Cerenkov counter, and Sergey Kuleshov will participate in the tracking system design and will improve the parameters of the Inner Calorimeter. Nikolay Pivnyuk and Ivan Bedlinsky are committed to significant contributions in the development of the CLAS12 software.

Summary

We plan to study electroproduction of π^0 and η mesons with a proton target above the resonance region ($W > 2\,\mathrm{GeV}$), in the kinematics of high photon virtualities, Q^2, or/and high momentum transfer, t. In these regions meson production is expected to be dominated by the reaction with a single quark ("handbag graph") and can be interpreted in terms of the generalized parton distributions (GPDs) in the proton. The proposed experiment will for the first time access the region of both high Q^2 and high t. The aim of the measurements is to (a) explore the transition from the hadronic to the partonic regime by testing model-independent predictions of the partonic reaction mechanism, and by making measurements over a wide range of Q^2 and t; (b) to extract information about the polarized quark GPDs in the proton. The π^0 and η are identified by measuring the two decay photons. It is planned to measure both the L/T separated cross sections for a limited set of Q^2 values, as well as unseparated cross sections and response functions, via azimuthal angle dependence and beam spin asymmetries, over a wide range of Q^2. The proposed experimental technique is uniquely suited to the CLAS12 spectrometer. This experiment is part of the comprehensive program of measurements of exclusive electroproduction with CLAS12, in which various channels, such as DVCS and vector meson production will be measured simultaneously.

I. INTRODUCTION

Exclusive electroproduction processes $\gamma^*(Q^2) + N \rightarrow M + N$ ($M = \gamma, \text{meson}$) offer a unique opportunity to study the structure of the nucleon as one varies both the size of the probe — the photon virtuality, Q^2 — and the momentum transfer to the nucleon, t. Such processes can reveal much more information about the reaction dynamics and the structure of the target than either inclusive electroproduction (Q^2 only) or elastic form factors ($t = -Q^2$). One may broadly organize the possible measurements into three kinematic regions:

(1) Resonance region: $W < 2\ GeV$, low to high Q^2,

(2) Deep–inelastic region: $W > 2\ GeV$, high Q^2, low t,

(3) High–t region: $W > 2\ GeV$, high t, low to high Q^2.

Of particular interest is the fact that at large Q^2 and/or large t exclusive electroproduction can be described in terms of the quark degrees of freedom of QCD. In the limit of large Q^2 and W, and low t [the asymptotic regime of region (2)], QCD factorization theorems state that exclusive electroproduction of photons [1, 2] and mesons [3] is dominated by a mechanism in which the production process happens in the reaction of the virtual photon with a single quark in the nucleon ("handbag graph"). The information about the nucleon is contained in the generalized parton distributions (GPDs) [2, 4, 5], describing the emission and absorption of the active quark by the nucleon. Similarly, it has been argued that exclusive production of photons [6, 7] at large t [region (3)], and of mesons at large t and large Q^2 [8], effectively proceeds via a partonic mechanism, and can again be described in terms the GPDs in the nucleon. This opens the prospect of using exclusive electroproduction processes such as deeply–virtual Compton scattering (DVCS) and meson production as a means to systematically explore the quark structure of the nucleon. Measurements at 6 GeV beam energy have demonstrated the feasibility of such studies, and have furnished first tests of the partonic reaction mechanism. The full realization of this program is one of the major objectives of the 12 GeV upgrade of CEBAF and the upgrade of the CLAS spectrometer.

A unique feature of measurements with the CLAS12 spectrometer is that data for different final states (photons, mesons) in all three kinematic regions (1)–(3) will be taken simultaneously. This makes it possible to accumulate the high statistics necessary for a

precise measurement of exclusive channels. It also dictates a structure of experimental proposals somewhat different from that for dedicated experiments. Exclusive measurements in region (1) will be discussed as part of the baryon resonance program. Measurements of DVCS [region (2)] are the subject of a companion proposal.

The present proposal deals with the electroproduction of π^0 and η mesons above the resonance region ($W > 2\ GeV$), at high Q^2 [region (2)], and high t [region (3)]. The common aims of the measurements are:

- To explore the transition from the "hadronic" to the "partonic" reaction mechanism, by focusing on observables testing model-independent features of the reaction mechanism, and by making measurements over a wide range of Q^2 and t;
- To extract information about the quark structure (GPDs) of the nucleon by comparing the data with theoretical model calculations.

The high–Q^2 measurements of π^0 and η electroproduction are closely related to, and complement, the planned DVCS measurements with CLAS12. The high–t measurements complement and extend existing and planned measurements of wide–angle real Compton scattering and meson production. A region which can be accessed for the first time with the 12 GeV upgrade is electroproduction at both high Q^2 *and* high t, where meson electroproduction is expected to be dominated by a partonic mechanism [8]. Measurements in this unexplored region will significantly enhance our understanding of the partonic mechanism and the quark structure of the nucleon.

The electroproduction of π^0 and η mesons possesses a number of unique features which give it a special place in the extensive program of exclusive measurements planned with the 12 GeV Upgrade. Because the pseudoscalars are spin–0 hadrons, stable with respect to strong interactions, it is in many ways the simplest electroproduction process from the point of view of its amplitude structure. Precise data exist on π^0 and η photoproduction in the resonance region and at high W, which form borders of the region explored in the present experiment. In the partonic regime at high Q^2, pseudoscalar production probes the "polarized" GPDs in the nucleon [9, 10], which contain information about the spatial distribution of the quark spin which is difficult to isolate in DVCS alone; see Ref. [11] for a review. The partonic structure of the pion itself has extensively been studied in processes such as $\gamma^*\gamma \to \pi^0$ [12, 13], which are measured in e^+e^- annihilation experiments [14]. An

important point is also that π^0 and η production does not involve pion exchange in the t–channel; its t–dependence at small t is regular and can unambiguously be associated with the structure of the nucleon rather than its pion cloud.

The extraction of information about the quark structure of the nucleon (GPDs) from electroproduction data is a challenging problem, which requires a careful approach. A detailed understanding of the reaction mechanism (*e.g.*, corrections to the partonic mechanism from hadronic–size configurations in high–Q^2 production) is essential before one can meaningfully compare with theoretical calculations based on GPD models. We plan to address this problem by making detailed measurements of observables which test *model-independent features* of the reaction mechanism, such as t–slopes, flavor ratios, *etc.*, and, generally, by studying the variation of observables over a wide range of Q^2 and t (details will be given below). π^0 and η production, thanks to its simple amplitude structure, is an ideal place to perform such systematic studies. They should eventually be extended to other exclusive channels as well (vector meson production, DVCS).

This proposal is organized as follows. In view of the differences in the theory and phenomenology of high–Q^2 [region (2)] and high-t electroproduction [region (3)] we discuss the physics motivation for the measurements separately for the two kinematic regions, in Section II and III (this should not obscure the underlying unity of the phenomena studied here). Section IV discusses the experimental aspects and the results of our previous with the current version of CEBAF and CLAS. In Sec. V we present the projected experimental results with the upgraded CEBAF and CLAS12 based on extensive simulations.

II. PHYSICS AT HIGH Q^2, LOW t

Electroproduction of pseudoscalar mesons (π^0, η) at $|t| \lesssim 1\,\mathrm{GeV}^2$ exhibits a rich structure, with different reaction mechanisms governing different regions of W and Q^2 (see Fig. 1). Production at $W < 2\,\mathrm{GeV}$ is dominated by the excitation of nucleon resonances in the s–channel, most notably the Δ. Photoproduction at high energies ($W > 2\,\mathrm{GeV}$) is well described by t–channel exchange of Regge poles, with ω and ρ being the dominant trajectories, see Refs. [15, 16] for a review. Limited data exist on high–energy electroproduction at low Q^2 [17, 18], which indicate a sudden change in the reaction dynamics at around $Q^2 \sim m_\rho^2$; the nature of this transition is not fully understood within Regge phenomenology [19].

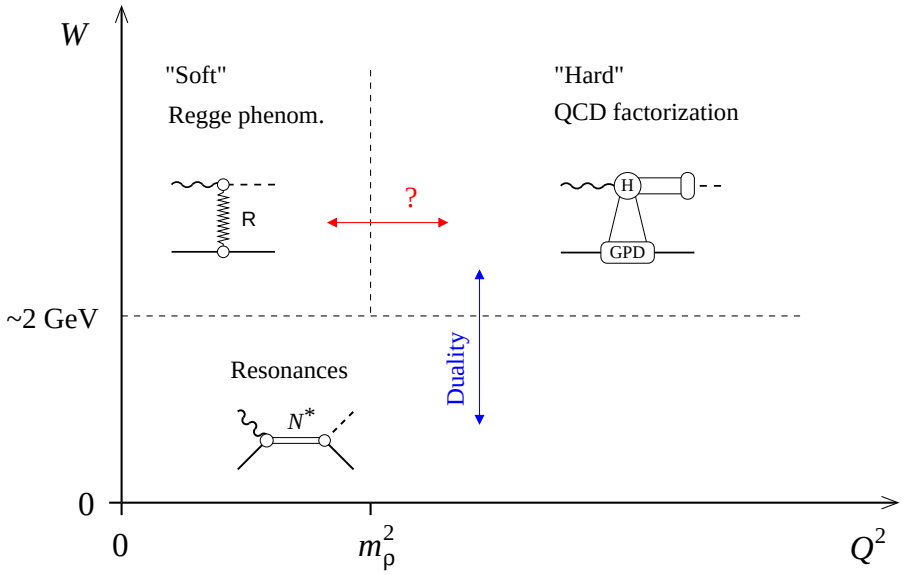

FIG. 1: The Q^2 and W "landscape" of pseudoscalar meson (π^0, η) electro/photoproduction at low t.

In the deep–inelastic limit of high W and high Q^2, a QCD factorization theorem states that meson production is dominated by the scattering from a single, quasi–free quark in the proton [3]. In the leading–twist approximation, *i.e.*, in leading order of $1/Q^2$, the amplitude for longitudinal photon polarization can be expressed as a convolution a hard scattering amplitude (describing the quark–level scattering process), the meson distribution amplitude (describing the hadronization of the outgoing quark/antiquark pair), and the generalized parton distributions in the proton (describing the emission/absorption of the "active" quark by the proton). The GPDs are universal, process–independent characteristics of the nucleon, which combine aspects of the usual parton densities with those of elastic form factors (see Fig. 2 for a summary). Their fascinating properties, and their potential for uniting traditional concepts of nucleon structure in a single QCD–based description, have been widely discussed in recent years; see Refs. [11, 20, 21] for a review of the extensive literature. In the case of pseudoscalar meson production the amplitude involves the axial vector–type GPDs, $\tilde{H}$ and $\tilde{E}$, whose moments are related to the axial and pseudoscalar nucleon form factors,

$$\int_{-1}^{1} dx\ \tilde{H}(x,\xi;t) \ = \ g_A(t), \tag{1}$$

$$\int_{-1}^{1} dx\ \tilde{E}(x,\xi;t) \ = \ h_A(t). \tag{2}$$

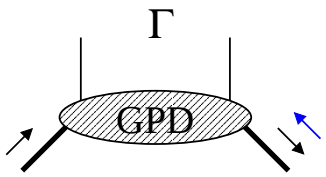

	nucleon helicity non-flip	nucleon helicity flip
$\Gamma = \gamma_\mu$	H	E
quarks unpolarized	Dirac	Pauli
$\gamma_\mu\gamma_5$	$\tilde{H}$	$\tilde{E}$
quarks polarized	Axial	Pseudoscalar

FIG. 2: GPDs as components of the (light-cone) quark density in the nucleon. The 4 independent structures reflect the number of quark distributions (unpolarized, polarized) times that of vector/axial vector form factors.

The GPDs $\tilde{H}$ and $\tilde{E}$ are closely related to the distribution of quark spin in the proton. The function $\tilde{H}$ reduces to the polarized quark/antiquark densities in the limit of zero momentum transfer,

$$\tilde{H}(x, \xi = 0; t = 0) \; = \; \begin{cases} \Delta q(x), & x \; > \; 0\,, \\ \Delta\bar{q}(-x), & x \; < \; 0\,. \end{cases} \tag{3}$$

Its Fourier transform with respect to t, the so–called impact parameter representation [22, 23] describes the transverse spatial distribution of quark spin in the proton — a property of fundamental interest for our understanding of the structure of the nucleon. The GPD $\tilde{E}$ describes the correlation of the quark spin distributions with the transverse momentum transfer to the nucleon; its value at zero momentum transfer is unknown and cannot be inferred from the quark densities themselves. We note that the flavor components of the GPDs entering in the π^0 and η production amplitudes are

$$\begin{aligned} \pi^0 : \quad & 2\Delta u - \Delta d, \\ \eta : \quad & 2\Delta u + \Delta d, \end{aligned} \tag{4}$$

where Δq stands for the polarized GPDs. By measuring the π^0 and η production cross section in the deep–inelastic region we can in principle extract information about the polarized GPDs in the proton, and thus the spatial distribution of quark spin, including its flavor dependence.

The physical idea underlying QCD factorization is that in the limit of large Q^2 the meson is produced in a small–size configuration in transverse space (transverse size $\sim 1/Q$). It is the coupling of these small–size configurations to the proton which is described by

the GPDs. In production processes at realistic values of Q^2, there will always be non-negligible contributions from configurations of normal hadronic size (transverse size $\sim R_{\rm pion}$). These contributions become relatively less important as Q^2 increases. In the context of the QCD expansion these contributions are referred to as higher–twist corrections; however, trying to describe them in terms of QCD degrees of freedom may not always be feasible. For experiments aimed at studying the approach to the partonic regime and extracting information about the GPDs, there are two basic strategies for dealing with this problem:

(a) Choose observables and kinematics to maximize the contribution from small–size configurations,

(b) Provide enough information for theoretical calculations to separate contributions from small–size and hadronic–size configurations.

Strategy (a) requires measurements at the highest possible Q^2, and observables which select longitudinal photon polarization. Strategy (b) requires measurements over a wide range of Q^2, W, and t, which allow one to observe systematic variations indicative of the transition from the hadronic to the partonic regime. The unique capabilities provided by the 12 GeV upgrade and the CLAS12 spectrometer make it possible to pursue both strategies at the same time.

The polarization of the virtual photon plays a crucial role in the transition from the soft to the hard regime. QCD factorization applies to the amplitudes for production by longitudinally polarized (L) photons, which dominate at large Q^2 [3]. The amplitudes for transversely polarized (T) photons can generally not be expressed in terms of GPDs. This is a consequence of the fact that longitudinal photons couple on average to configurations of substantially smaller transverse size than transverse ones. For testing the approach to the partonic reaction mechanism, and for extracting information about the GPDs, it is essential to separate contributions from L and T photons to the cross section. The differential cross section for pseudoscalar meson production involving polarized electrons is given by

$$\begin{aligned}\frac{d\sigma}{d\Omega^*} &= \sigma_T + \epsilon\sigma_L + \epsilon\sigma_{TT}\cos 2\phi^* \\ &+ \sigma_{LT}\sqrt{2\epsilon(\epsilon+1)}\cos\phi^* + h\sqrt{2\epsilon(\epsilon+1)}\sigma_{LT'}sin\phi^*, \end{aligned} \tag{5}$$

where ϵ is the virtual photon polarization, h the beam helicity, and σ_L, σ_T, σ_{LT} and σ_{TT} are structure functions which depend on Q^2, W and t. The most direct way to isolate the L

photon contribution is by way of Rosenbluth separation of σ_L and σ_T. This requires combination of measurements at different beam energies at the same Q^2, which appears feasible for a limited number of Q^2–values up to about $6\,(\mathrm{GeV}/c)^2$. The unseparated cross sections can be measured up to $10\,(\mathrm{GeV}/c)^2$. Much more information on the relative importance of longitudinal and transverse amplitudes can be obtained by measuring the interference structure functions σ_{TT} and σ_{LT} via the azimuthal angle dependence of the cross section, and $\sigma_{LT'}$ via the single–spin asymmetry, which can be done over a wide range of Q^2, W and t. The study of the Q^2–dependence of these function will provide crucial tests of the approach to the hard mechanism.

The first aim of the proposed experiment is to explore the transition from the soft to the hard regime in π^0 and η electroproduction above the resonance region. Here we focus on observables testing features of the reaction mechanism, which are free from the uncertainties of present model calculations (related to the modeling of the GPDs, treatment of the hard scattering process *etc.*). In many cases we can perform the same test using both L/T separated cross sections (to be measured over a limited range of Q^2) and unseparated ones (to be measured accurately over a wide range of Q^2, W and t); the two methods nicely complement each other, adding to the leverage of our conclusions.

- *Q^2–dependence of cross sections.* The simplest test of the approach to the hard reaction mechanism is provided by the Q^2–dependence of the differential cross sections. QCD factorization predicts that the hard contribution to the (dominant) longitudinal cross section drops as $1/Q^6$, while the soft contributions to the longitudinal cross section, as well as the various transverse cross sections, drop at least as $1/Q^8$. We plan to test this prediction in the following ways:

  - Measure the unseparated differential cross section and see if it approaches a $1/Q^6$ behavior;
  - Measure the ratio σ_L/σ_T and see how fast it decreases with Q^2;
  - Measure the interference cross sections σ_{TT} and σ_{LT} via the azimuthal angle dependence, and $\sigma_{LT'}$ via the single–spin asymmetry, and compare their Q^2–dependence to that of the unseparated cross section.

Figure 3 shows the η production cross section measured in the E16 experiment at 6

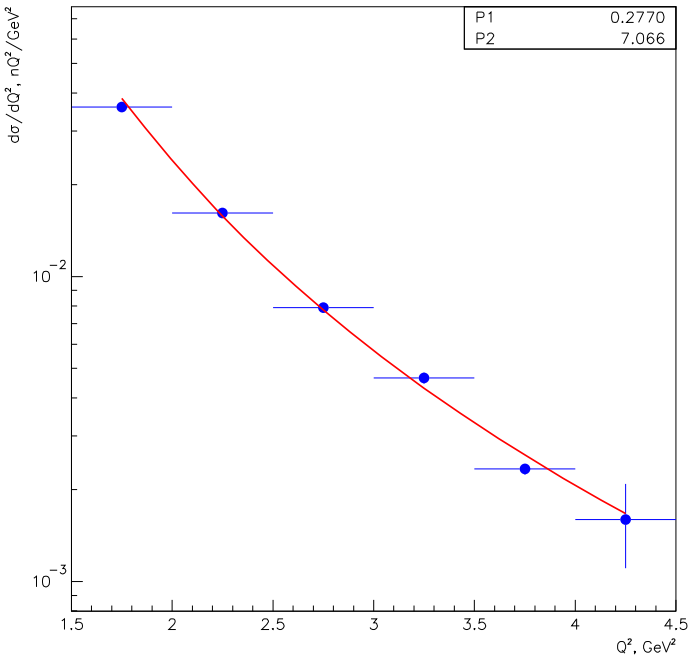

FIG. 3: The η meson electroproduction cross section, measured in the E16 experiment at 6 GeV, as a function of Q^2. The Q^2–dependence is consistent with that implied by the hard production mechanism, $1/Q^8$. Note that the plot shows the electroproduction rather than the virtual photon cross section, containing an additional factor $1/Q^2$.

GeV; the data already seem to consistent with the power behavior implied by the hard mechanism.

- *t–dependence and its change with Q^2.* Another prediction of the hard reaction mechanism is that the t–dependence of the amplitude originates solely from the GPD. This immediately follows from the fact that the meson is produced in a configuration of small transverse size, $\sim 1/Q$, whence the transverse size of the interaction region is determined by the structure of the target alone (see Fig. 4). As a result, the t–slope of the cross section in the forward peak should become independent of Q^2, and two production processes probing the same GPD at the same x–values should exhibit identical t–slopes. This test has been applied with great success to diffractive production of vector mesons at small x, where the data show that the t–slopes of $J/\psi, \phi$ and ρ meson production all converge to the same value, $B \approx 5\,\mathrm{GeV}^{-2}$, at $Q^2 \gtrsim 10\,\mathrm{GeV}^2$,

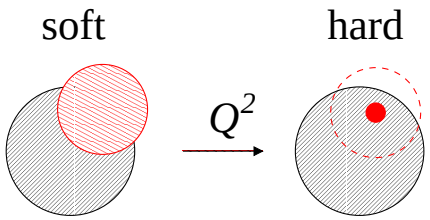

FIG. 4: The transverse spatial structure of meson electroproduction. At $Q^2 = 0$, the meson is produced in a configuration of "normal" hadronic transverse size. At large Q^2, the longitudinal cross section is dominated by configurations of transverse size $1/Q$. The t–slope of the differential cross section measures the overall size of the interaction region, and thus allows one to test the dominance of small–size configurations.

reflecting the t–dependence of the gluon GPD (see Fig. 5) [24, 25]. In π^0 and η electroproduction in our experiment, we can perform similar tests of the dominance of small–size configurations in a variety of ways:

- Measure the t–slope of the unseparated differential cross section, $d\sigma/dt$, in the forward peak; check if it decreases with Q^2 and becomes stable at large Q^2. Fig. 6 shows the Q^2–dependence of the t–slopes for η production measured in the E16 experiment, up to large values of t. The data indeed show a decrease of the t–slope with increasing Q^2, consistent with the approach to the hard scattering mechanism. Note, however, that the slope shown here is an effective slope over a broad region of t; more precise data in the forward peak ($|t| \lesssim 1\,\mathrm{GeV}^2$) are needed in order to decide whether the small observed value, $B \sim 1\,\mathrm{GeV}^{-2}$, is due to the small size of the probe or the small effective transverse size of the target at large x.
- Measure the t–slopes of $d\sigma_L/dt$ and $d\sigma_T/dt$ separately. On general grounds one expects that L has a smaller t–slope than T, and that the L slope approaches a constant value at large Q^2 earlier than the unseparated cross section.
- Compare the t–slopes of π^0 and η production as a function of Q^2. To the extent that both reactions are dominated by the u–quark GPD in the proton, *cf.* Eq. (4), they should exhibit the same t–slopes at high Q^2.
- Measure the "dip structure" of the differential cross sections, including the inter-

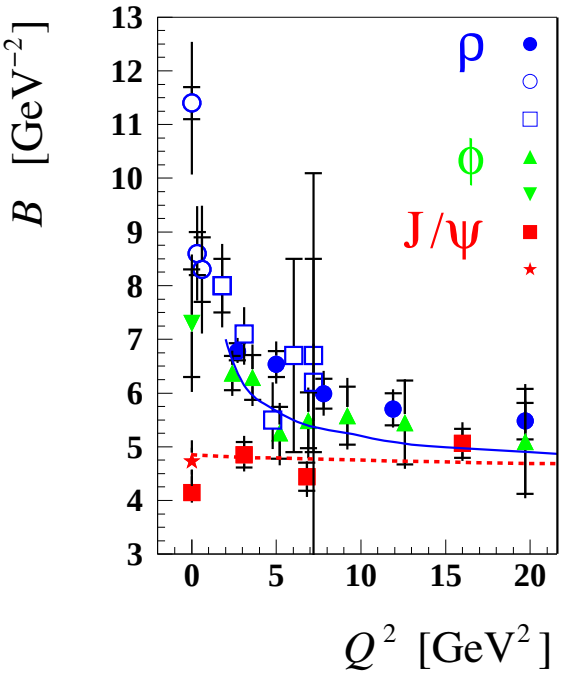

FIG. 5: The slope parameter, B, for ρ (blue), ϕ (green) and J/Ψ (red) photo/electroproduction measured by HERA H1 and ZEUS, as a function of Q^2 [24, 25]. The data show the convergence of all t–slopes to a universal value at large Q^2, indicating that the mesons are produced in point–like configurations.

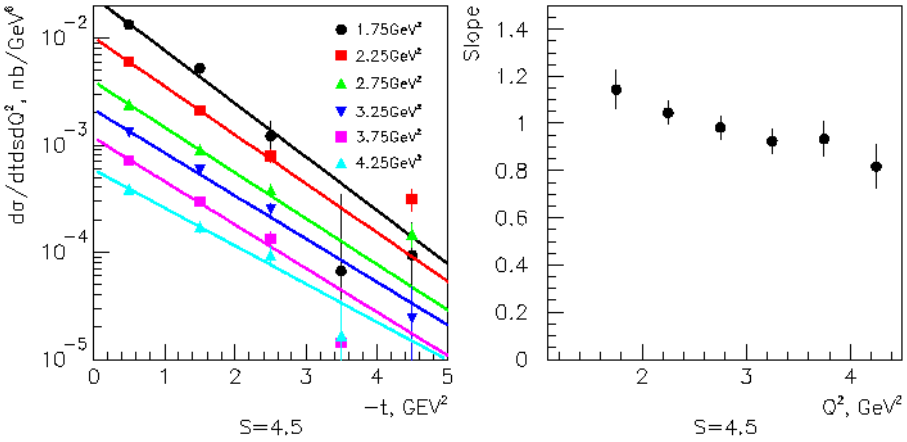

FIG. 6: The t–dependence of the differential cross section for η meson electroproduction for various Q^2. The left panel shows the t–dependence of the data, the right panel the exponential t–slope as a function of Q^2.

ference cross sections σ_{TT}, σ_{LT} and $\sigma_{LT'}$, and see how it evolves with Q^2. This is a particularly interesting observable to study the transition from the Regge regime at low Q^2 to the hard regime at high Q^2. In simple Regge pole exchange, the dip structure is dictated by properties of the Regge trajectories and should not change with Q^2 [26]. A Q^2–dependence of the dips at small Q^2 ($\sim 1\,\mathrm{GeV}^2$) would therefore indicate a deviation from simple Regge pole exchange [19, 27].

When interpreting the observed t–slopes and their Q^2–dependence in terms of a transverse spatial size of the interaction region, we need to take into account that the value of $t_{\min}$ changes with Q^2. The relevant variable is really the transverse momentum transfer to the proton, $-\boldsymbol{\Delta}_\perp^2$, which differs from t by a Q^2–dependent amount. This effect is usually neglected at small x but may become significant at JLab energies. The ensuing modifications in the spatial interpretation of the t–slopes are presently under theoretical investigation.

- *W–dependence of cross sections.* Another interesting observable testing the reaction mechanism is the energy dependence of the cross section at fixed, high values of Q^2. QCD factorization states that the longitudinal cross section dominates in the high–Q^2, high–W region. When we approach this region from low W, we therefore expect the longitudinal cross section to rise faster with energy than the transverse one. Furthermore, we expect the W–dependence of the cross section to become steeper with increasing Q^2. In the asymptotic regime this should happen due to the effect of Q^2–evolution on the GPDs. While we are in a regime where QCD evolution may not be applicable literally, it is interesting to see if this property holds in a "duality" sense. We thus propose to

  - Measure the W–dependence of σ_L and σ_T at fixed high Q^2; see if σ_L rises faster than σ_T.
  - Compare the W–dependencies of σ_L at fixed high Q^2; see if it becomes steeper with increasing Q^2.

- *Flavor relations.* In neutral pseudoscalar meson production the hard reaction mechanism implies some interesting model–independent relations between the ratio of the amplitudes for π^0, η and η' production [28]. They follow from the "universality" of

the GPDs — production processes with the same t–channel quantum numbers involve the same GPD — and the relations between the pseudoscalar meson wave functions imposed by $SU(3)$ flavor symmetry and the $U(1)$ axial anomaly of QCD. In the case of exact $SU(3)$ symmetry in the pseudoscalar sector, Ref. [28] predicts a ratio of $\pi^0 : \eta : \eta'$ cross sections of

$$\frac{1}{2}\left(\frac{2}{3}\Delta u + \frac{1}{3}\Delta d\right)^2 \;:\; \frac{1}{6}\left(\frac{2}{3}\Delta u - \frac{1}{3}\Delta d + \frac{2}{3}\Delta s\right)^2 \;:\; \frac{1}{3}\left(\frac{2}{3}\Delta u - \frac{1}{3}\Delta d - \frac{2}{3}\Delta s\right)^2, \tag{6}$$

where Δu, Δd, and Δs are the polarized quark densities in the proton. Assuming $\Delta d \approx -\Delta u$ and $\Delta s = 0$, this implies a ratio of $\pi^0 : \eta : \eta' = 1{:}3{:}6$. This prediction changes to 1:4.8:4.3 if the effect of $SU(3)$ symmetry breaking and the $U(1)$ axial anomaly are taken into account. We also note that for coherent production from a deuteron target the $SU(3)$ symmetric estimate is $\pi^0 : \eta : \eta' = 27{:}1.6{:}1.4$, completely reversing the relative order of π^0 and η. We plan to test the flavor relations for the proton target:

- Measure the $\pi^0 : \eta$ cross section ratio as a function of Q^2, both for the longitudinal cross sections and for the unseparated cross sections, which are expected to be dominated by σ_L at large Q^2.

The second, more ambitious aim of the proposed experiment is to utilize the data on π^0 and η electroproduction at high Q^2 to extract quantitative information about the polarized GPDs, and thus about the spatial distribution of quark spin in the proton. In this part of the investigation we necessarily have to rely at least partly on model calculations of the production amplitudes.

Present model calculations of the leading–twist contribution to pseudoscalar meson production amplitudes suffer from considerable theoretical uncertainties [29], caused both by the shortcomings of present ansätze for the GPDs, and by the uncertainties in the treatment of the hard scattering process (*e.g.* the choice of QCD scale). With the presently available data this uncertainty could not really be reduced by comparing with the data, since the relative importance of leading and higher–twist contributions in the data remained unclear. We expect a significant improvement of the situation with the data from the proposed experiment. The new data will extend our knowledge of longitudinal as well as unseparated cross sections to substantially higher Q^2 and W, where the leading–twist contribution becomes

more clearly visible. Even more important, the numerous tests of the reaction mechanism described above, and the detailed mapping of the Q^2 dependence of longitudinal as well as transverse cross sections, will allow us to tune phenomenological models containing both leading and higher–twist contributions, making it possible to extract information about the twist–2 contribution. A promising starting point for developing such models is the space–time picture of the production process [30], in which one can separate contributions from small–size ($\sim 1/Q$) and hadronic–size ($\sim 1/R_{\rm pion}$) contributions. In diffractive scattering at high energies, such "two–component" models successfully describe the ρ meson production data down to $Q^2 \sim$ few GeV^2, where they exhibit significant higher–twist effects [31].

An important technique in extracting quantitative information about the GPDs will be to compare different production channels in the same kinematics. In this way we can make statements about certain *relative* properties of the GPDs, which are largely independent of model assumptions and the details of the hard scattering process. For example, we plan to

- Compare the measured t–slopes of π^0 and η production (which probes the polarized quark GPDs, $\tilde{H}$ and $\tilde{E}$) with that of ρ^+ production (which probes the unpolarized quark GPDs, $\tilde{H}$ and $\tilde{E}$). In this way we can extract information about the relative transverse sizes of unpolarized and polarized quark distributions in the proton. It is generally expected that the polarized quark distributions are concentrated at smaller transverse distances than the unpolarized ones. The comparison with the t–slope of ρ^0 production, which involves also the gluon GPD, will reveal information about the relative transverse size of the quark and gluon distributions in the proton. Detailed model predictions for the transverse spatial distribution of quarks and gluons exist, which can be tested in this way.

- Compare the cross sections and t–dependence of π^0 and η production with that of π^+ production. The latter process involves t–channel pion exchange, which in the GPD formalism appears in the form of a pion pole contribution to the helicity–flip GPD, $\tilde{E}$ [10, 32]. It is generally assumed that this pion pole contribution dominates over the regular part of the GPD in π^+ production; this assumption is crucial for experiments which attempt to extract the charged pion form factor from the electroproduction data [33]. In neutral pion electroproduction the pion pole is absent on grounds of charge conjugation invariance. By comparing π^0 and π^+ production, we can now

quantitatively test the hypothesis of pion pole dominance in $\tilde{E}$. In addition to being of interest for our understanding of the quark structure of the nucleon, this will put the charged pion form factor analysis on a solid footing.

The t–dependence of the GPDs, and its correlation with the x– and ξ–dependence, has been extensively discussed in the last two years, and is considered by many theorists to be one of the most interesting aspect of these distributions. It has become clear that the assumption of factorization of the x–and t–dependence,

$$\tilde{H}(x,\xi;t) \;\; = \;\; f(x,\xi)\; g(t), \tag{7}$$

which was used in early model calculations, is strongly violated both at $x \to 1$ and at small x. The t–slope of the GPD, and thus the effective transverse size of the nucleon, is expected to increase with decreasing x. Various parametrizations have been proposed for the correlated x– and t–dependence of the GPDs. For example, Ref. [34] proposes a simple ansatz

$$\tilde{H}(x,\xi=0;t) \;\; = \;\; \Delta q(x)\; \exp\left[t\, \tilde{f}(x)\right], \tag{8}$$

where

$$\tilde{f}(x) \;\; = \;\; \alpha' \log(1/x) + (A-\alpha')(1-x) \tag{9}$$

describes the correlation of the x– and t–dependence, exhibiting Regge–like behavior at small x (first term) and a vanishing slope at $x \to 1$ due to the "Feynman mechanism" (second term). Extended parametrizations for $\xi \neq 0$ have also been discussed in the literature [11]. With the expected data on π^0 and η production we can constrain the parameters in these parametrizations, and thus extract information about the transverse spatial distribution of quark spin in the proton ("nucleon tomography").

A special feature of π^0 and η electroproduction is that it probes only non-singlet GPDs, which do not mix with gluons under QCD evolution — in contrast to DVCS and vector meson production, which involve singlet GPDs. The non-singlet GPDs are much less scale– and renormalization scheme dependent than the singlet ones, which greatly simplifies the QCD analysis of our processes. They are also much easier to compare with the results of non-perturbative model calculations, which makes them clean probes of the quark structure of the proton.

We stress again that π^0 and η production discussed in the present proposal represents only one component of the extensive program of exclusive electroproduction measurements planned with CLAS12, and that the GPD analysis will, of course, include information from other channels such as DVCS and vector meson production.

The proposed measurements require clean identification of the reactions $\gamma_V p \to p\pi^0$ and $\gamma_V p \to p\eta$ by way of detection of two photons from the meson decay, in addition to the scattered electron and the recoil proton. Experience with our experiments at $E_\gamma = 5.75$ GeV show that this is quite feasible and simulations at projected $E_\gamma = 11$ GeV indicate that this technique is admirably suited to CLAS12. In particular, we expect reasonable rates for π^0 and η production at the higher Q^2 values. Details of the simulations will be presented in Section V.

III. PHYSICS AT HIGH t

Exclusive production processes at high t probe the structure of the target at small impact parameters ($b \sim 1/\sqrt{-t}$). Next to elastic form factors, such processes are the main source of information about the short–distance structure of the nucleon. Of particular interest are measurements in the region of both high t *and* high Q^2, which probe the nucleon structure at small transverse distances with a small–size probe. This combination can be achieved for the first time with the proposed setup at 11 GeV.

The theoretical description of high–t processes in QCD is generally considered to be more challenging than that of high–Q^2 processes, where the photon virtuality defines an "external" short–distance scale. In the strict asymptotic limit of large t, the elastic and Compton form factors of the proton are dominated by the so–called hard scattering mechanism, in which all three valence quarks participate in a hard reaction involving the exchange of two hard gluons [35]. However, it is almost certain that this mechanism is not relevant at momentum transfers of the order of $|t| \sim$ few GeV. Instead, it has been argued that elastic and Compton form factors at realistic momentum transfers are dominated a "soft" mechanism [6, 7], in which the electromagnetic process happens via the interaction with a single quark ("handbag graph"), whose emission and absorption by the nucleon is described by GPDs. The amplitude for wide–angle real Compton scattering (WACS) can be expressed in terms of certain integrals

over the GPDs,

$$R_V(t) = \int_0^1 \frac{dx}{x}\, H(x,\xi=0;t) \tag{10}$$

$$R_A(t) = \int_0^1 \frac{dx}{x}\, \tilde{H}(x,\xi=0;t). \tag{11}$$

This approach describes well the s and t–dependence of the WACS cross section, and in particular the polarization transfer, K_{LL}, measured in the Hall A experiment [36]. It has been suggested that the same mechanism also be at work in meson electroproduction (in particular, π^0 and η) at high t and $Q^2 \sim$ few GeV^2 [8, 37]. The only difference to WACS is that an additional hard scattering process (gluon exchange) is required to form the outgoing meson, analogous to factorization in high–Q^2 electroproduction. The meson production amplitudes can be expressed in terms of the same GPD–related form factors (11) as in Compton scattering. In particular, π^0 and η production is dominated by the axial form factor, R_A, involving the polarized GPD, $\tilde{H}$.

The GPDs describing the amplitudes for high–t Compton scattering and meson production are the same basic functions as those probed in high–Q^2, low–t electroproduction; however, here they are evaluated at high t, where their behavior and physical significance may be quite different from that at low t. Still, it is extremely valuable that one has a unified description of high–Q^2 and high–t electroproduction on the basis of QCD degrees of freedom. In particular, it is possible to use information from high–t Compton scattering and meson electroproduction to extract information about the GPDs in the proton. We note that high–t exclusive processes have also been studied in an extension of Regge phenomenology (originally considered in photoproduction at high W, small t), using the concept of saturating Regge trajectories [26].

The aim of the proposed measurements at high t is to test the reaction mechanism for high–t pseudoscalar meson electroproduction (π^0 and η) and to probe the structure of the nucleon at short distances. In particular, we plan to explore for the first time the region of both high t and high Q^2, where pseudoscalar meson electroproduction is expected to be governed by the "handbag" mechanism, and the π^0 and η data can be interpreted in terms of the GPDs in the proton.

As in high–Q^2 electroproduction, in the first step we first focus on observables which test largely model–independent aspects of the reaction mechanism for π^0 and η production. Specifically, these are:

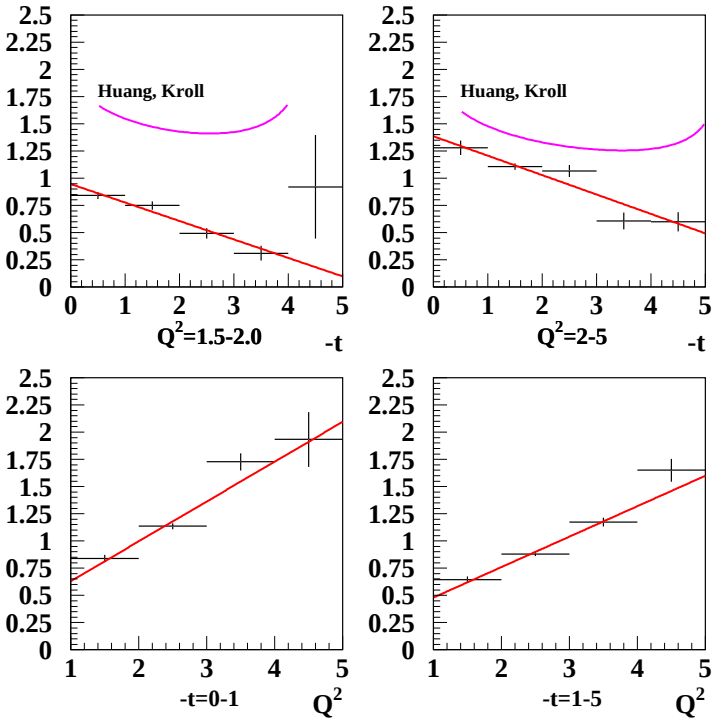

FIG. 7: The ratio of the differential cross sections for η and π^0 production as a function of t for two Q^2–bins (top row), and as a function of Q^2 for two t–bins (bottom row). The purple lines show the predictions from the model of Ref. [8] based on the handbag mechanism.

- *s–dependence of cross section.* A basic prediction of the handbag mechanism is that the differential cross section at fixed angle drops approximately as s^{-7}. This behavior is obtained assuming that the form factors, $R_V(t)$ and $R_A(t)$, drop approximately as $1/t^2$, which follows from a generic wave function overlap picture. In particular, it will be interesting to see how the large–s behavior changes between photoproduction and $Q^2 \sim 2-3\,\mathrm{GeV}^2$. Finite Q^2 should reduce contributions from the hadronic structure of the photon (vector–meson dominance–type), which have a faster fall–off with energy. One should thus expect the s^{-7} to become effective earlier at higher Q^2. Also, it will be interesting to compare the s–dependence of π^0 and η production with that of wide–angle real Compton scattering, which in the handbag approach is predicted to be $\sim s^{-6}$.

- *Absolute cross sections as function of Q^2.* The handbag mechanism alone greatly underestimates the differential cross section for the π^0 and η photoproduction data at

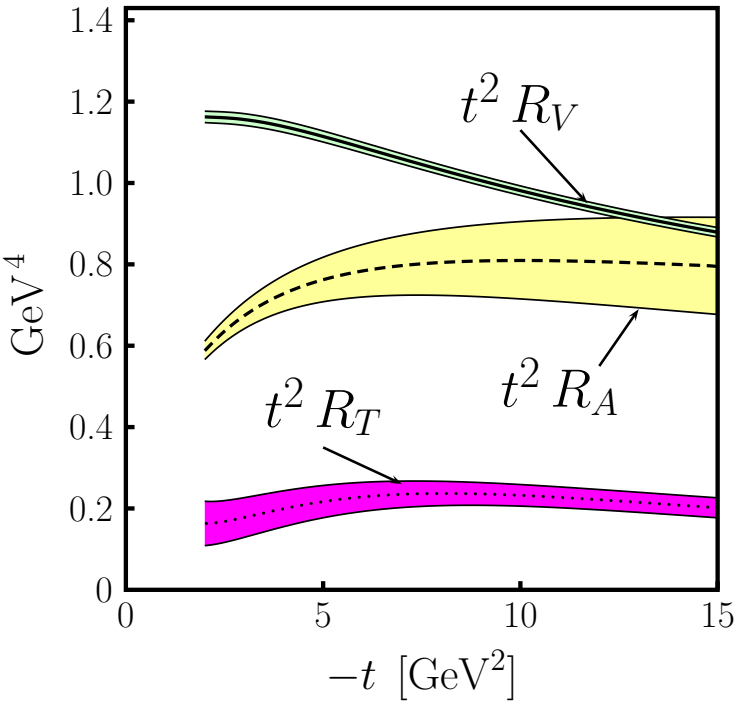

FIG. 8: The Compton form factors, R_V and R_A, extracted from fits to the present form factor and wide–angle real Compton scattering data [34]. The axial form factor, R_A, can be measured in π^0 and η electroproduction at high t and high Q^2.

high t. This is explained by the fact that the dominant contribution to photoproduction at $|t| \sim$ few GeV^2 comes from the hadronic structure of the photon. It is expected that already moderate values of $Q^2 \sim 2-3\,\mathrm{GeV}^2$ will suppress this contribution, leaving the handbag mechanism the dominant player. If this is correct, one should observe in the description of the absolute cross section by the handbag formula with standard parameters with increasing Q^2.

- *Flavor relations.* As in electroproduction at high Q^2, the ratio of π^0 and η production cross section is a more robust prediction of the handbag mechanism than the individual absolute cross sections, since it is practically independent of the modeling of the hard scattering process (one–gluon exchange). The E1-6 data indicate that the measured ratio rapidly approaches the handbag prediction with increasing Q^2 (see Fig. 7).

- *L/T ratio.* As in high–Q^2 electroproduction, the dominant contribution to the cross section at high t and $Q^2 \sim$ few GeV^2 in the handbag approach is expected to come from L photon polarization. We can test this prediction by studying the Q^2 dependence of

the L/T ratio in large–t electroproduction. Additional information will come from the measurement of the interference cross sections σ_{TT}, σ_{LT} and $\sigma_{LT'}$.

If the tests confirm the relevance of the handbag mechanism, one can compare the data with quantitative predictions for the form factors R_A obtained from models of the high–t GPDs. In particular, it will be interesting to perform a combined analysis of the data for wide–angle real Compton scattering and high–t electroproduction of π^0 and η mesons within the handbag approach. π^0 and η production is dominated by the axial form factor, R_A, while Compton scattering probes mainly the vector form factor, R_V. Figure 8 shows the uncertainty in the extraction of R_A from the present data on axial form factors and wide–angle real Compton scattering [34]. With the expected data on π^0 and η production at high t and high Q^2 we expect to significantly reduce this uncertainty. In this way we can obtain valuable information about the quark structure of the nucleon at small distances, which complements the information obtained from elastic form factor measurements at high t.

IV. RESULTS FROM JLAB EXPERIMENTS E1-6 E01-113 AND RELEVANCE TO THIS PROPOSAL

Experiment e1-6 measured electroproduction of vector mesons, pseudoscalars mesons, and photons (DVCS) over a wide kinematic region. The ρ and ω results have been already published [38, 39]. Preliminary data on pseudoscalar meson production, while still under analysis, have been presented at various conferences [40]. The distribution of the π^0 and η production cross sections over Q^2, W, and t measured in this experiment have already provided crucial information about the approach to the partonic reaction mechanism (see Sections II and III) are an essential input for our projections for measurements with CLAS12 at 11 GeV. In this section we briefly describe the experience with the experimental apparatus and analysis technique gained from the e1-6 experiment, as relevant to the present proposal, and summarize the results on π^0 and η production.

The e1-6 experiment was completed during the period November 2001–January 2002. We used a 5.75 GeV longitudinally polarized electron beam with an average polarization of

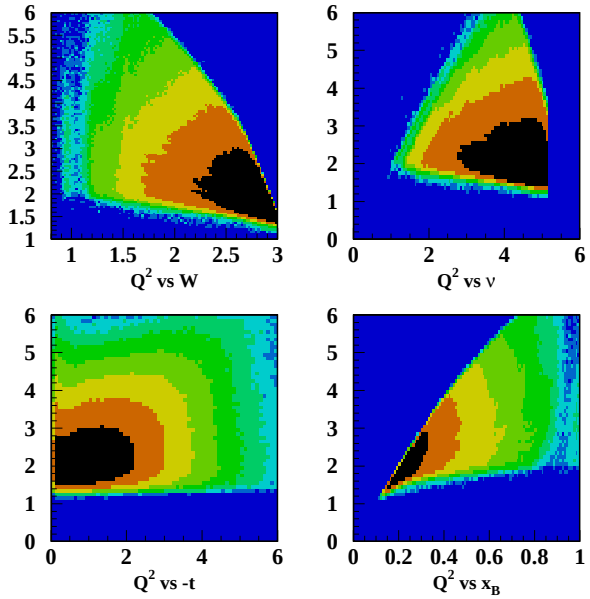

FIG. 9: The kinematic coverage of the e1-6 experiment. Top left panel: Q^2 vs W. Top right panel: Q^2 vs ν. Bottom left panel: Q^2 vs $-t$. Bottom right panel: Q^2 vs x_B.

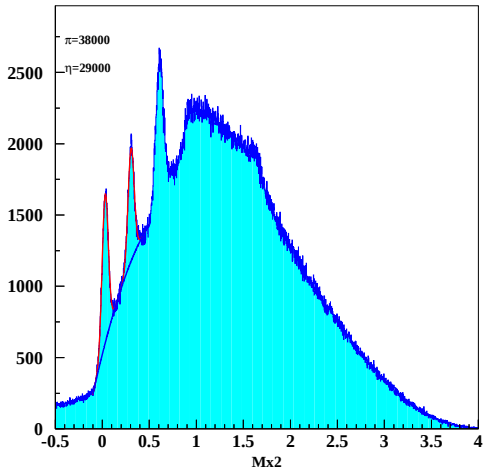

FIG. 10: Missing mass^2 distribution in the reaction $ep \to epX$ with $W > 2$ GeV cut.

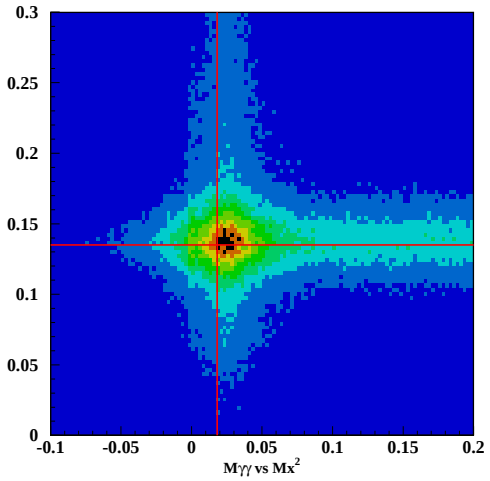

FIG. 11: The $M_{\gamma\gamma}$ vs Mx^2 distribution in the reaction $ep \to ep\gamma\gamma$ with $W > 2$ GeV cut. The π^0 peak is clearly seen.

$\sim$ 80%, incident on the 5 cm long liquid hydrogen target. A total of 3.7x10^9 electron events were collected during data taking. The coincidence signal of the forward electromagnetic calorimeter (EC) and the Cherenkov counter (CC) was used as a data acquisition a trigger. Fig. 9, shows the kinematic coverage in Q^2, x_B, W, and t for reconstructed electron-proton pairs from the preliminary analysis of the collected data.

The missing mass^2 distribution in the reaction $ep \to epX$ is presented in Figs. 10 and 11. One clearly sees the peaks in the spectrum corresponding to γ–π^0, η, and ρ–ω production.

For the proposed experiment at 11 GeV the identification of π^0 and η mesons by missing mass is not feasible, since at higher energies the missing mass resolutions become progressively poorer. Thus, we plan to identify and characterize the π^0 and η production by detection of their decay photons. The recently run experiment E01-113 utilized a new highly segmented calorimeter similar to the inner calorimeter which will be used in CLAS12. Our experiences in detecting the η and π^0 decays via $\vec{e}p \to ep\gamma\gamma$ are extremely useful for obtaining a prognosis of what we can expect with CLAS12. The inner calorimeter (IC) detected high-energy photons in the angular range from 4 to 16 degrees. The setup also employed a new superconducting solenoid magnet to shield the CLAS drift chambers (DC) and IC from Møller electrons. The same type of simulation as used in this CLAS12 proposal were very successful at describing the background in the IC, which originated mostly from Moller electrons. As anticipated, only the inner crystal layer suffered form significant pile-up and exhibited a small gain loss over a three-month period. Experiment E01-113 ran at the design luminosity of 2×10^{34} cm^{-2}sec^{-1}, which was limited primarily by instantaneous rates and current in the drift chambers.

In the present proposal, the magnetic field configuration will be different, with a strong field extending further away, and the IC located at a larger distance from the target. The success in simulating the background in E01-113 gives us confidence in the simulations for the present proposal.

A. IC performance

Energy resolution. The calorimeter was calibrated using two-cluster events from $\pi^0 \to \gamma\gamma$ [41]. The obtained mass resolution of 7 MeV (σ) translates into an energy resolution of 4.5% for 1 GeV photons. With additional information from simulation [42] and from preamplifier noise, our quantitative estimate of the energy dependence of the resolution is

$$\frac{\sigma_E}{E}(\%) = \frac{1.9}{E} \oplus \frac{3.3}{\sqrt{E}} \oplus 2.4 \tag{12}$$

When extrapolated to 6-9 GeV photons, the resolution will be dominated by the constant term.

Position resolution. The intrinsic IC position resolution, as estimated from simulation [42]

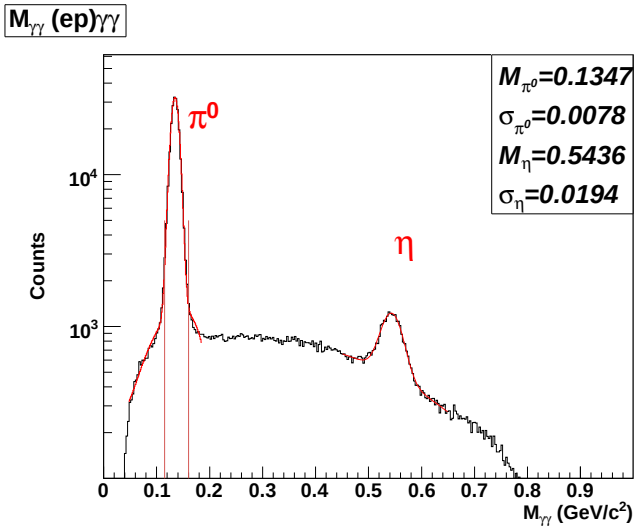

FIG. 12: The $\gamma\gamma$ invariant mass spectra from the IC calorimeter.

and compatible with present data, is

$$\sigma_x = \sigma_y(\text{mm}) \simeq \frac{1.8}{\sqrt{E}} \oplus 0.1 \tag{13}$$

This will translate into .2 mrad resolution for a 9 GeV photon for a point target viewed from a distance of 1.75 m.

Time resolution. After electron flight path correction and time-walk correction, a resolution of 0.7 ns was obtained in the $e-\gamma$ coincidence. This is dominated by the multihit-TDC channel width of 0.5 ns. This resolution may be used to reject the few remaining accidentals in the CLAS-IC coincidence.

The $\gamma\gamma$ invariant mass spectra from the inner calorimeter is shown in Fig.12. π^0 and η peaks are clearly seen in the spectrum.

B. Preliminary results

After calibration of all detector subsystems and particle identification cuts for the scattered electron and proton, the selection of the $ep \to ep\gamma\gamma$ events is straightforward. The $ep \to ep\gamma\gamma$ events were selected by requiring a good electron, a proton and two photons above 0.5 GeV. Figure 15 summarizes the preliminary results for the one-dimensional (integrated over all other kinematic variables) distributions of the cross section: $d\sigma/ds$ ($s = W^2$), $d\sigma/dt$, and $d\sigma/dQ^2$ for the reaction $ep \to ep\eta$. We note that the hard reaction mechanism

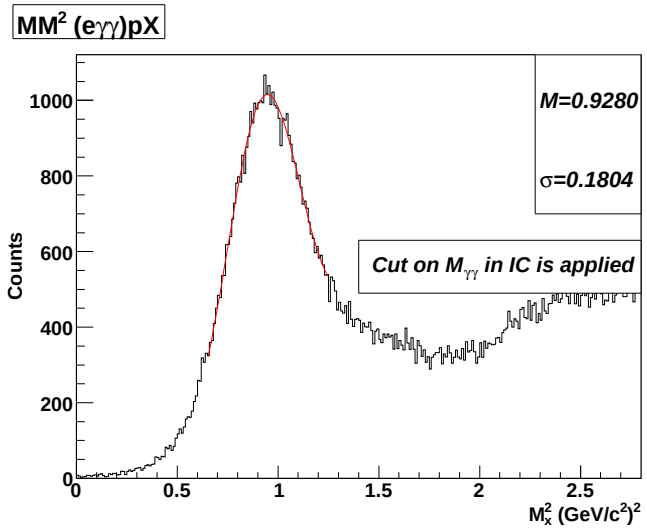

FIG. 13: The missing mass spectrum in the reaction $ep \to e\gamma\gamma X$ after the cut $M_{\gamma\gamma} = M_{\pi^0} \pm 2\sigma$. The proton peak is clearly seen.

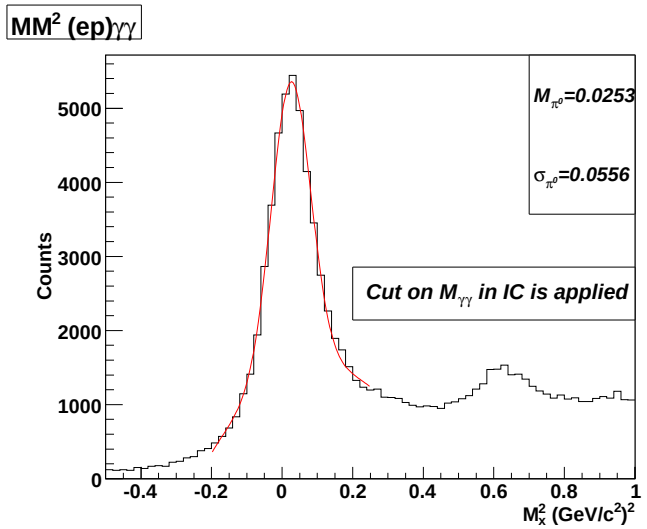

FIG. 14: The missing mass spectrum in the reaction $ep \to epX$ after the cut $M_{\gamma\gamma} = M_{pi^0} \pm 2\sigma$. The π^0 peak is clearly seen.

predicts a Q^2 behavior of the cross section as $d\sigma/dQ^2 \sim 1/Q^n$, with $n = 8$. It is interesting that the effective power fall-off corresponding to the lower curve in Fig. 15 is $n \approx 7$, rather close to this value. This is at least a qualitative indication that we may be approaching the hard regime.

Figure 16 shows the differential cross section $d\sigma/dtdsdQ^2$ for the reaction $ep \to ep\eta$ in the kinematic regions with $s = W^2 = 4.5, 5.5, 6.5$, and $7.5\,\mathrm{GeV}^2$. The data clearly show the

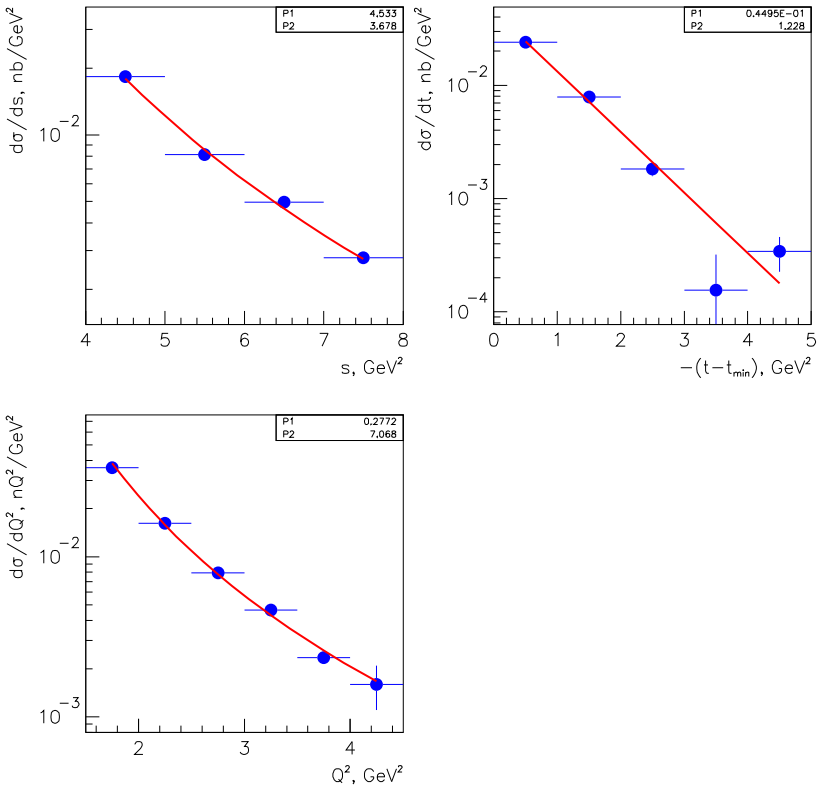

FIG. 15: $d\sigma/ds$, $d\sigma/dt$, and $d\sigma/dQ^2$ for the reaction $ep \to ep\eta$.

decrease of the t–slopes with increasing Q^2, corresponding to a decrease of the transverse size of the interaction region. Again, this is qualitatively consistent with the approach to a hard scattering regime. An exponential fit to these data gives slope parameters of the order of $B \sim 1\,\mathrm{GeV}^{-2}$, much smaller than typical hadronic sizes. Figure 17 illustrates the change of the t dependence with Q^2, and of the Q^2–dependence with t, in a different way. The top panels shows the effective exponent in a power–law fit to the t–dependence, $d\sigma/dt \sim 1/(-t)^n$, as a function of Q^2; the bottom panels the corresponding exponents of the Q^2–dependence as a function of t. These results clearly demonstrate the approach to a regime of small transverse size of the interaction region, fundamental to the hard scattering mechanism. Similar plots of the data from the e1-6 experiment and their implications have already been discussed in Sections II and III, see Figs. 3, 6 and 7.

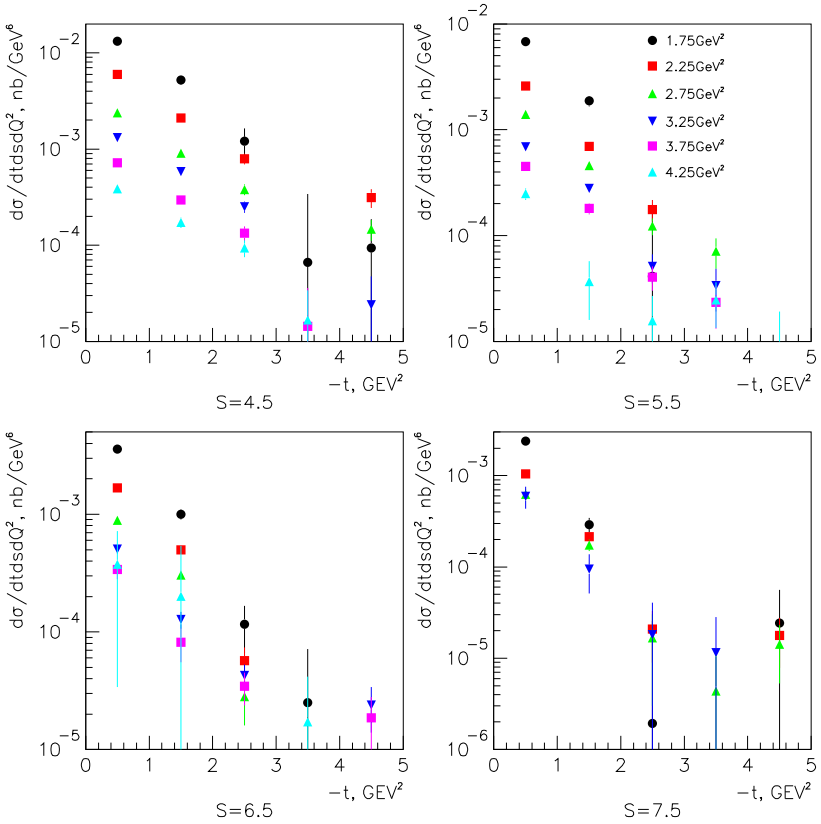

FIG. 16: $d\sigma/dtdsdQ^2$ for the reaction $ep \to ep\eta$ in the different kinematic regions with $s = W^2$=4.5, 5.5, 6.5, and 7.5 GeV^2.

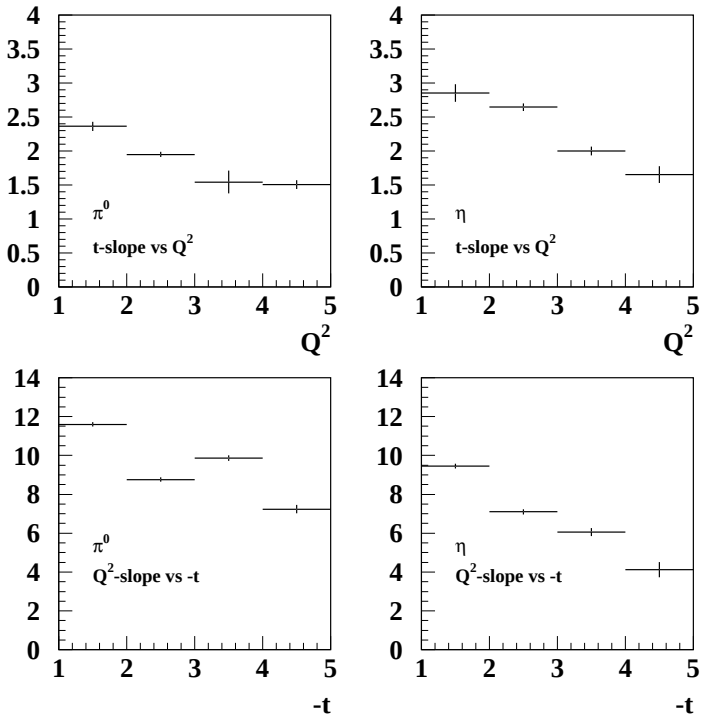

FIG. 17: The dependence of the slope parameters as a function of Q^2 and t. The top panels are the dependence of t slope parameters as a function of Q^2. The t-distribution was fitted by a power law function $d\sigma/dt \sim 1/(-t)^n$. The left panel is for the π^0 production, and right panel for η production. The bottom panels are the dependence of the Q^2 slopes n as a function of t. The Q^2-distribution was fitted by the function $d\sigma d/dt \sim 1/Q^n$. The left panel is for π^0 production, and right panel is for η production.

V. SIMULATIONS FOR THE CLAS12 PROPOSAL

A. Monte Carlo simulation

CLAS12 acceptances and projected data for the $ep \to e'p\pi^0$ and $ep \to e'p\eta$ reactions were estimated via Monte-Carlo simulations using the software package *FastMC*. *FastMC* employs a set of cuts in the coordinate and momentum spaces to represent the detector acceptance. These cuts are combined with parameterizations of the detector response from the various components of CLAS12. The efficiency of the active detector volumes is considered to be one. The event generator for the projected differential x_B and t dependencies of the cross sections is based on the GPD formalism. The total π^0 and η cross sections were extrapolated from the recent CLAS e1-6 data.

Exclusive π^0 and η events at the beam energy of 11 GeV were simulated in the range of 1 GeV$< Q^2 <$ 10 GeV, and 1 GeV$< -t <$ 10 GeV. Events at the beam energies of 8.8 GeV and 6.6 GeV were also simulated for the σ_L and σ_T separation. These events were passed through *FastMC* to simulate the detector response, and then acceptance-corrected to extract differential cross sections. Fig. 18 shows the kinematic landscape for the accepted event distributions, and Fig. 19 shows the accepted event distributions for each variable integrated over the other variables. For the purpose of rate estimates, events were generated assuming an experimental run of 1000 hours, which are shown in Fig. 19. Note that the expected rates are quite substantial even at the higher values of Q^2 and $-t$.

The various kinematic distributions, acceptances, and expected statistics in different kinematic regions for the π^0 and η productions are presented in the Appendix.

B. Response functions vs Q^2, x_B and t.

An important part of the experiment will be to extract the response functions in Eq. 5 as functions of Q^2, x_B and t. This will require the detailed knowledge of the acceptances as functions of these variables and ϕ^*. Fig. 20 shows an example of the CLAS12 acceptances for the π^0 channel as a function of ϕ^* at $-t = 1$ GeV^2 for different values of Q^2 and x_B. Fig. 21 shows the CLAS12 acceptances for the π^0 channel at $x_B = 0.5$ GeV^2 and $Q^2 = 6$ GeV^2 for different $-t$ bins.

To demonstrate the analysis procedure and its accuracy for the proposed measurement of

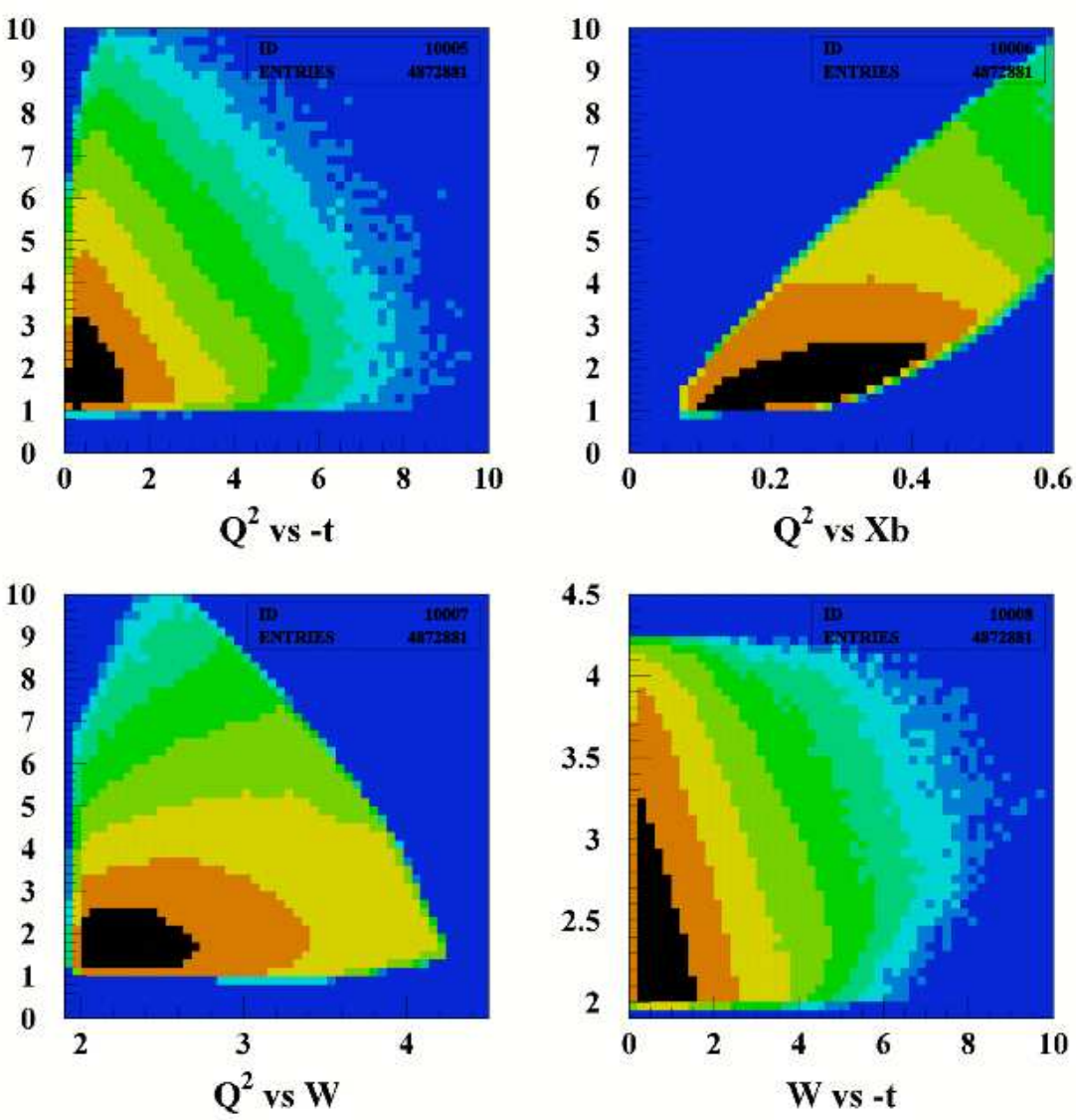

FIG. 18: Monte Carlo simulation of the reaction $ep \to ep\pi^0$. The x_B, Q^2, W, and t distributions for the accepted events.

response functions, events were generated according to Eq. 5 with $\sqrt{2\epsilon(\epsilon+1)}\sigma_{LT}/\sigma = 0.2$, $\epsilon\sigma_{TT}/\sigma = 0.05$, and $\sqrt{2\epsilon(\epsilon+1)}\sigma_{LT'}/\sigma = 0.1$ where $\sigma \equiv \sigma_T + \epsilon\sigma_L$. These were fed through *FastMC* to obtain the simulated detector "data". The "data" were acceptance-corrected to obtain the differential cross sections. These cross sections were then fit by a function of $A(1 + Bcos2\phi + Ccos\phi)$, where A, B, and C are related to the structure functions, $\sigma_T + \epsilon\sigma_L$, σ_{TT} and σ_{LT}, respectively as shown in Eq. 5. The fits to the acceptance corrected events for each bin for Q^2= 2 and 8 GeV^2 are shown in Figs. 22 and 23. Beam spin asymmetries are also simulated by measuring $(N^+ - N^-)/(N^+ + N^-)$ for each bin where $N^{\pm}$ are the number

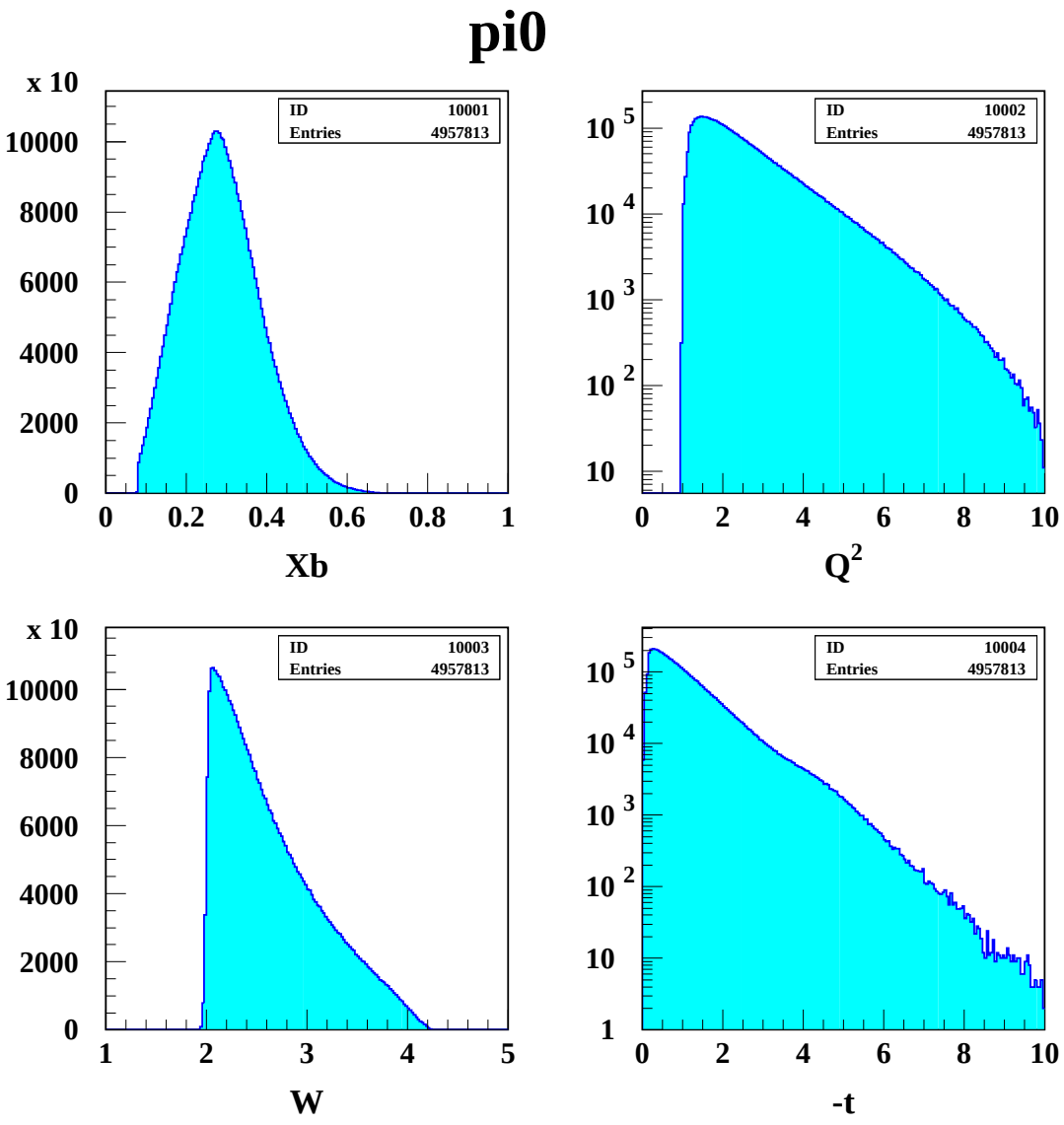

FIG. 19: Reaction $ep \to ep\pi^0$. Monte Carlo simulation. The x_B, Q^2, W, and t distributions for the accepted events integrated over the remaining variables.

of events from $\pm$ electron helicity state. These asymmetries were then fit by a function of $Asin\phi/(1 + Bcos2\phi + Ccos\phi)$ where A is related to $\sigma_{LT'}$. The fits to the simulated asymmetries for Q^2= 2 and 8 GeV^2 are shown in Figs. 24 and 25.

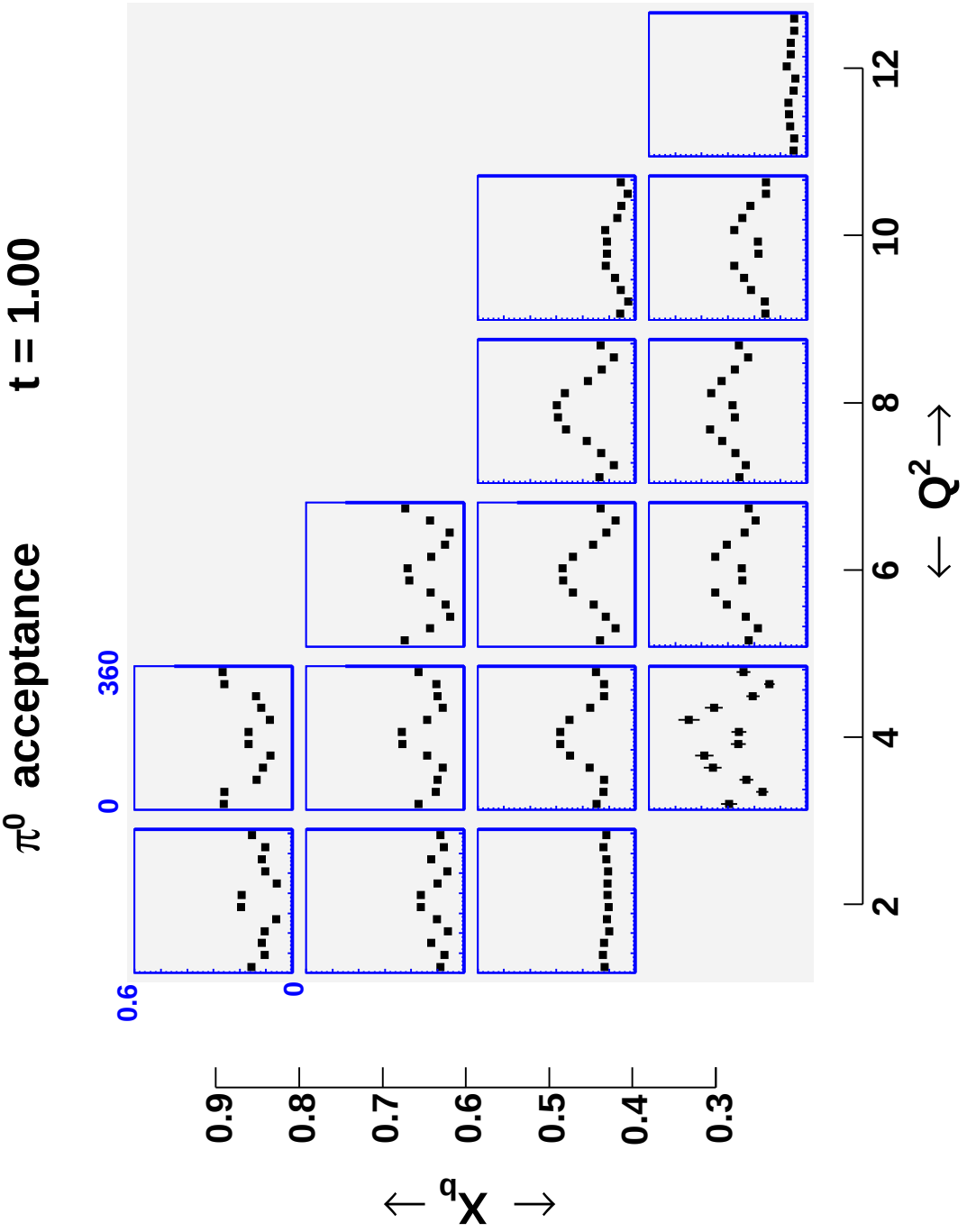

FIG. 20: Reaction $ep \to ep\pi^0$, $\pi^0 \to \gamma\gamma$. The CLAS12 acceptance as a function of x_B, Q^2, and ϕ for the events with electron, proton and two gammas are detected. t=1 GeV^2

C. Extraction of σ_T and σ_L

The extraction procedure detailed in the previous section yields $\sigma_T + \epsilon\sigma_L$, σ_{TT}, σ_{LT} and $\sigma_{LT'}$. To further separate σ_T and σ_L, we use the Rosenbluth L/T separation procedure. σ_T

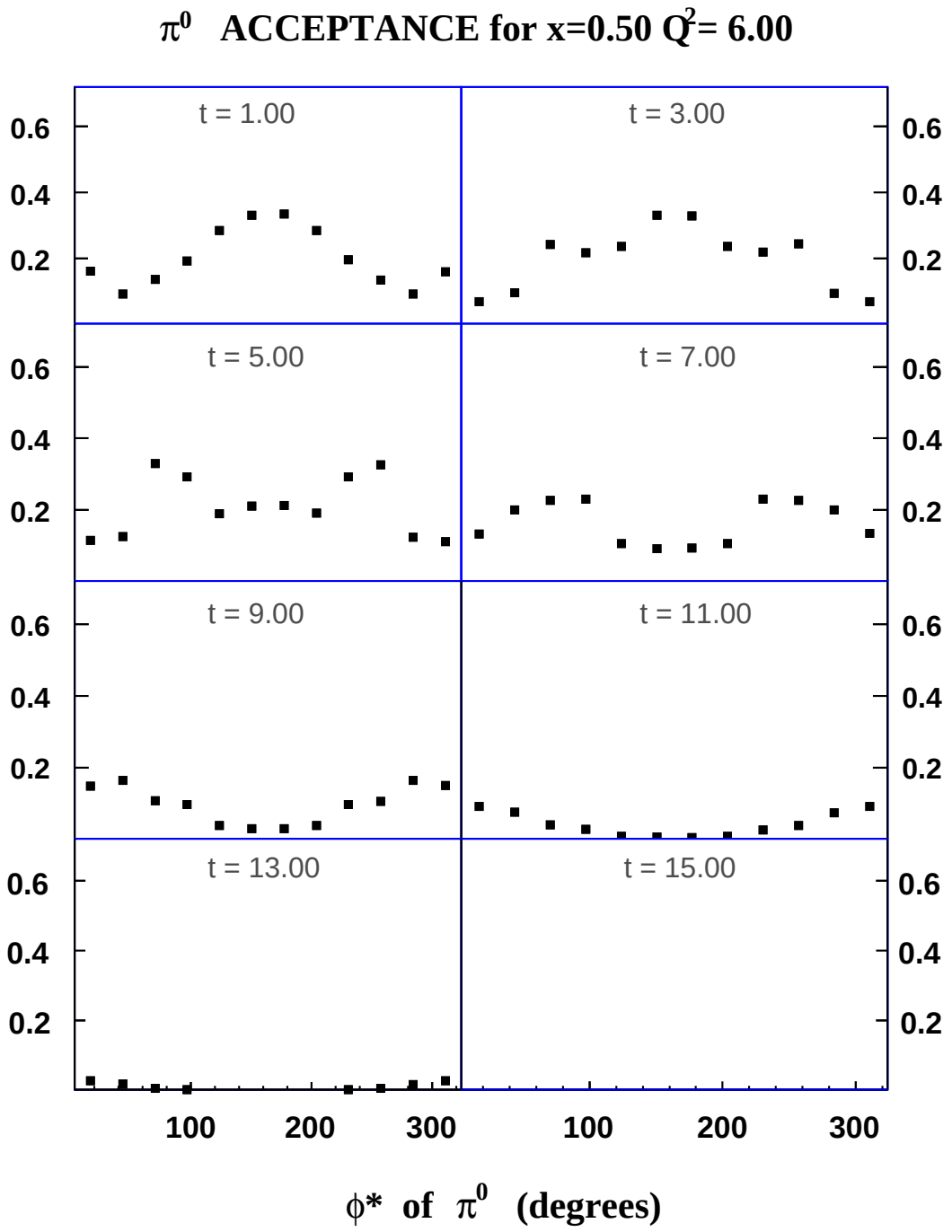

FIG. 21: Reaction $ep \to ep\pi^0$, $\pi^0 \to \gamma\gamma$. The CLAS12 acceptance as a function of ϕ for the events with electron, proton and two gammas are detected. x_B=0.5, Q^2=6 GeV^2

and σ_L depend on the variables Q^2, x_B and t, and ϵ represents the usual virtual photon polarization parameter. To perform the Rosenbluth procedure, it is necessary to vary ϵ by keeping Q^2 and x_B fixed, which can only be done by varying the beam energy. In this proposed experiment, we will use 6.6, 8.8 and 11 GeV incident beams. Fig. 26 shows the

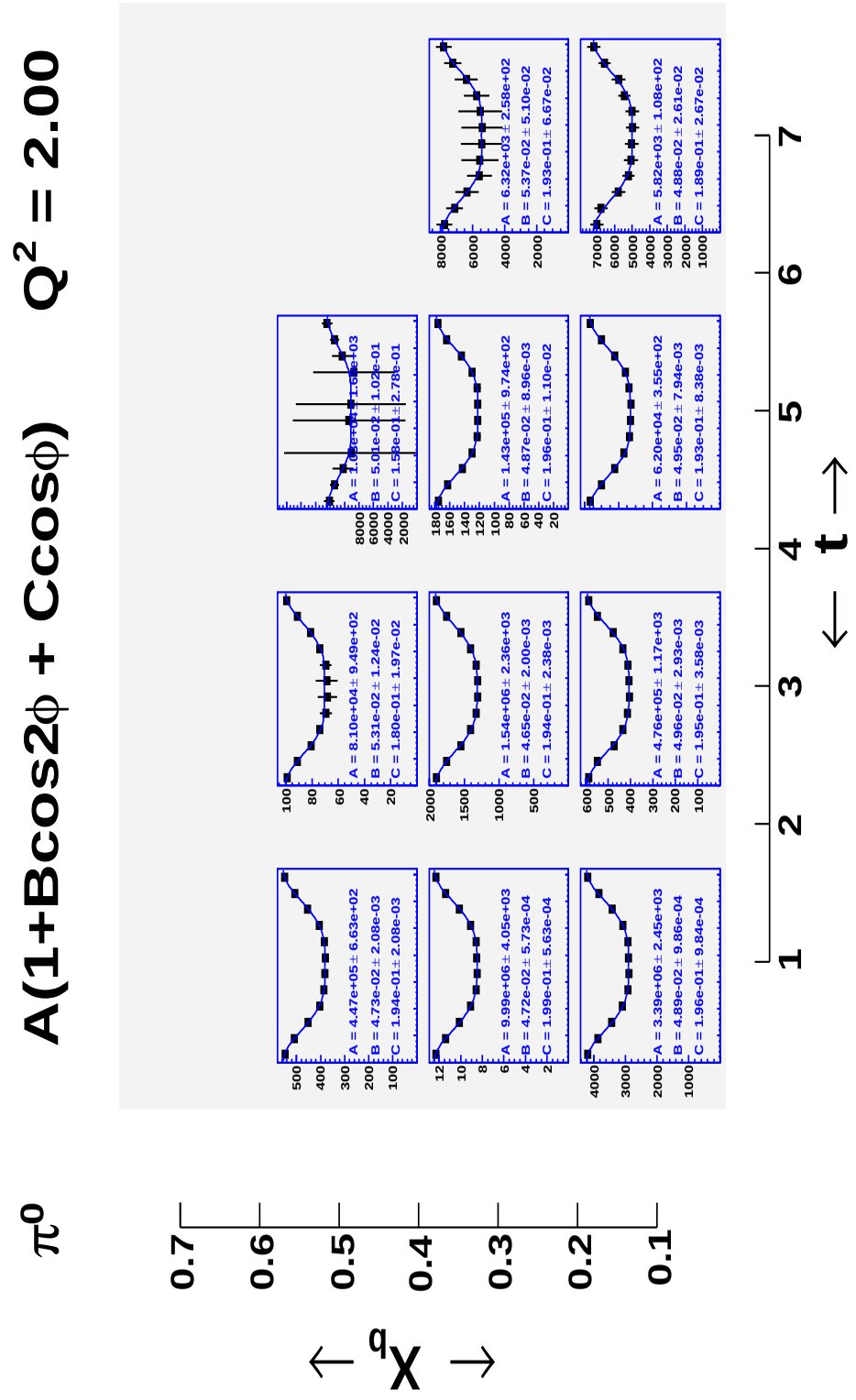

FIG. 22: Simulated cross sections for the reaction $ep \to ep\pi^0$, $\pi^0 \to \gamma\gamma$. The data were fit with the function $A(1 + Bcos2\phi + Ccos\phi)$ to obtain the parameters A, B and C

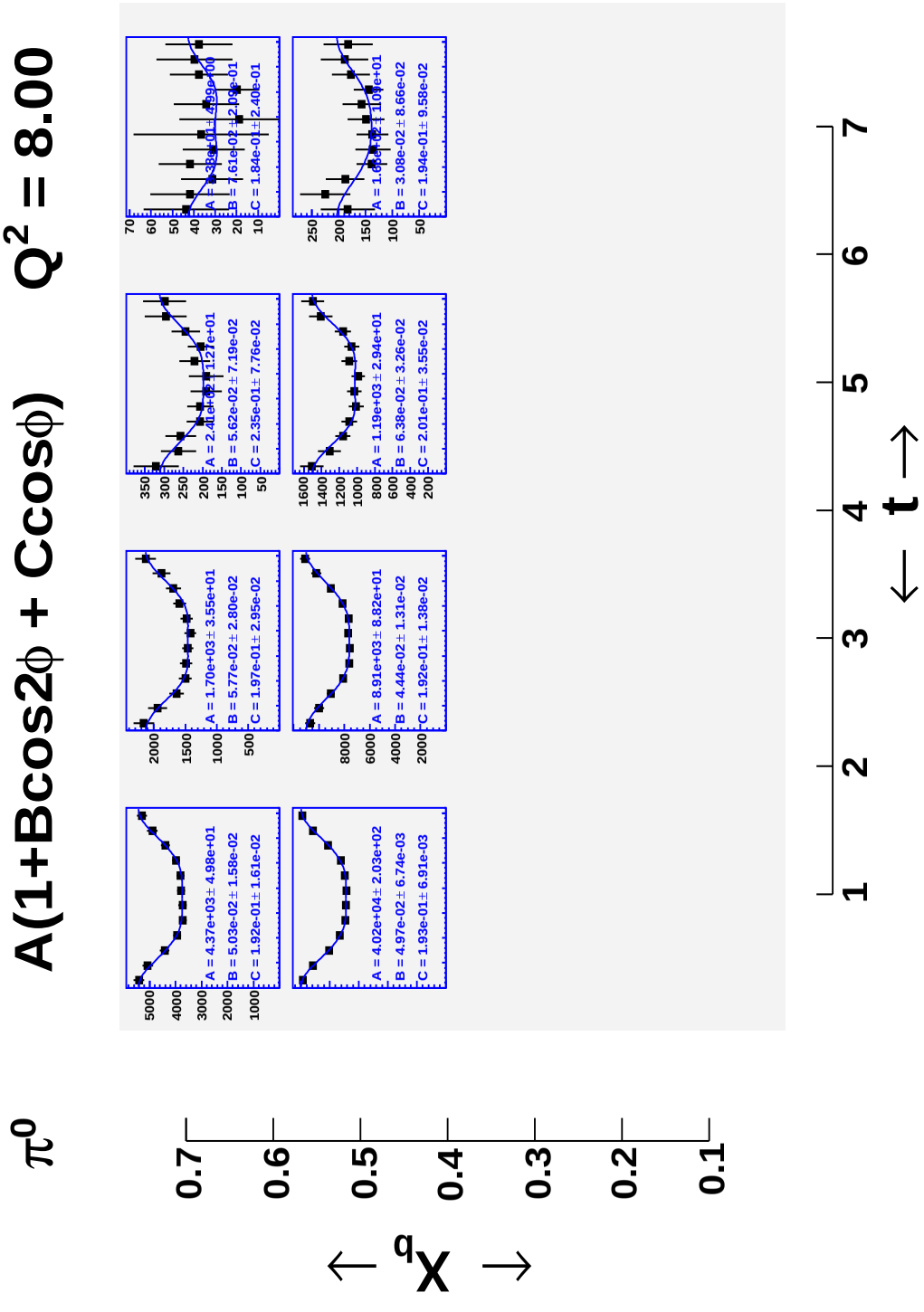

FIG. 23: Simulated cross sections for the reaction $ep \to ep\pi^0$, $\pi^0 \to \gamma\gamma$. The data were fit with the function $A(1 + Bcos2\phi + Ccos\phi)$ to obtain the parameters A, B and C

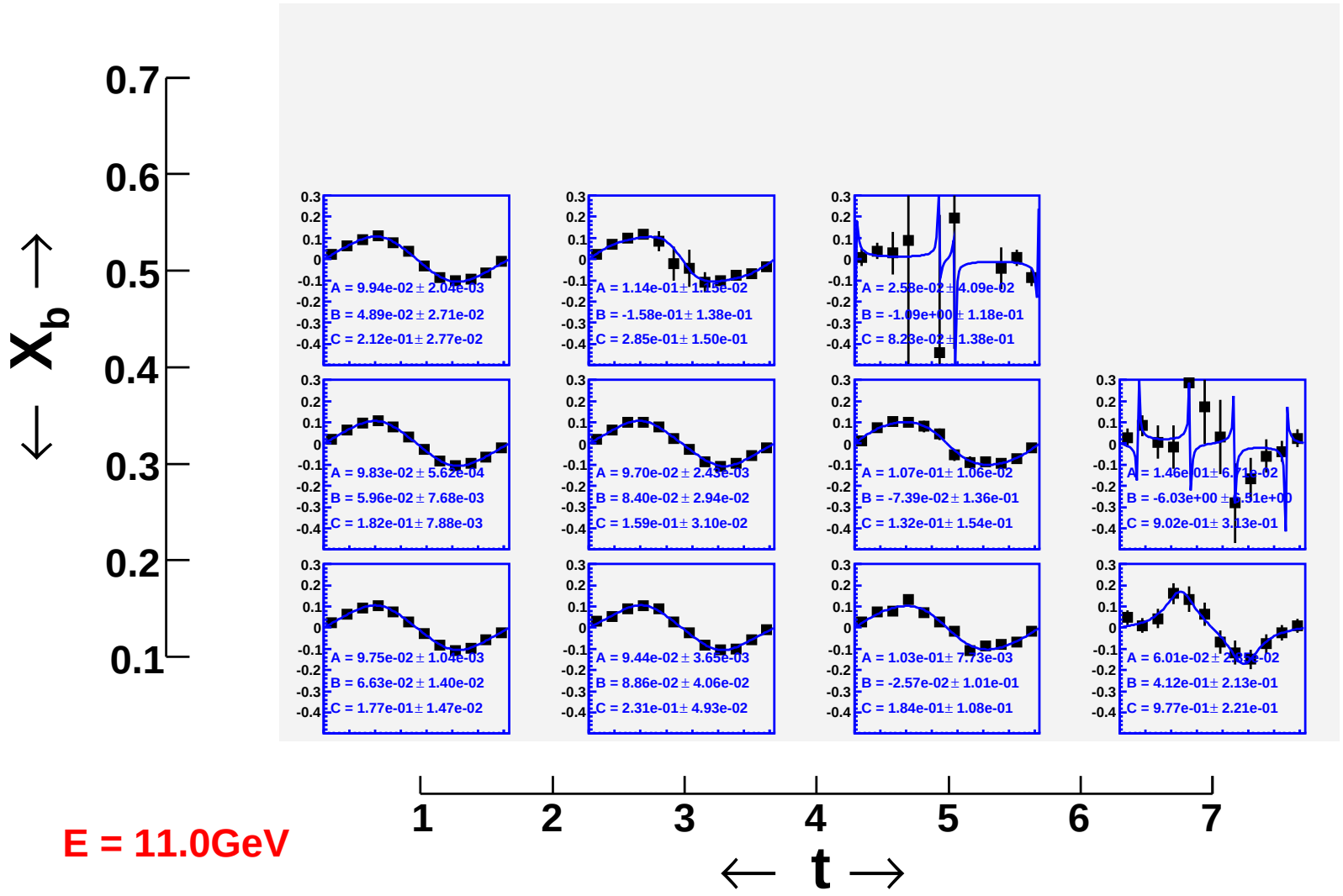

FIG. 24: Simulated asymmetries $A\sin\phi/(1+B\cos 2\phi+C\cos\phi)$ for the reaction $ep \to ep\pi^0$, $\pi^0 \to \gamma\gamma$ at $Q^2 = 2\ GeV^2$..

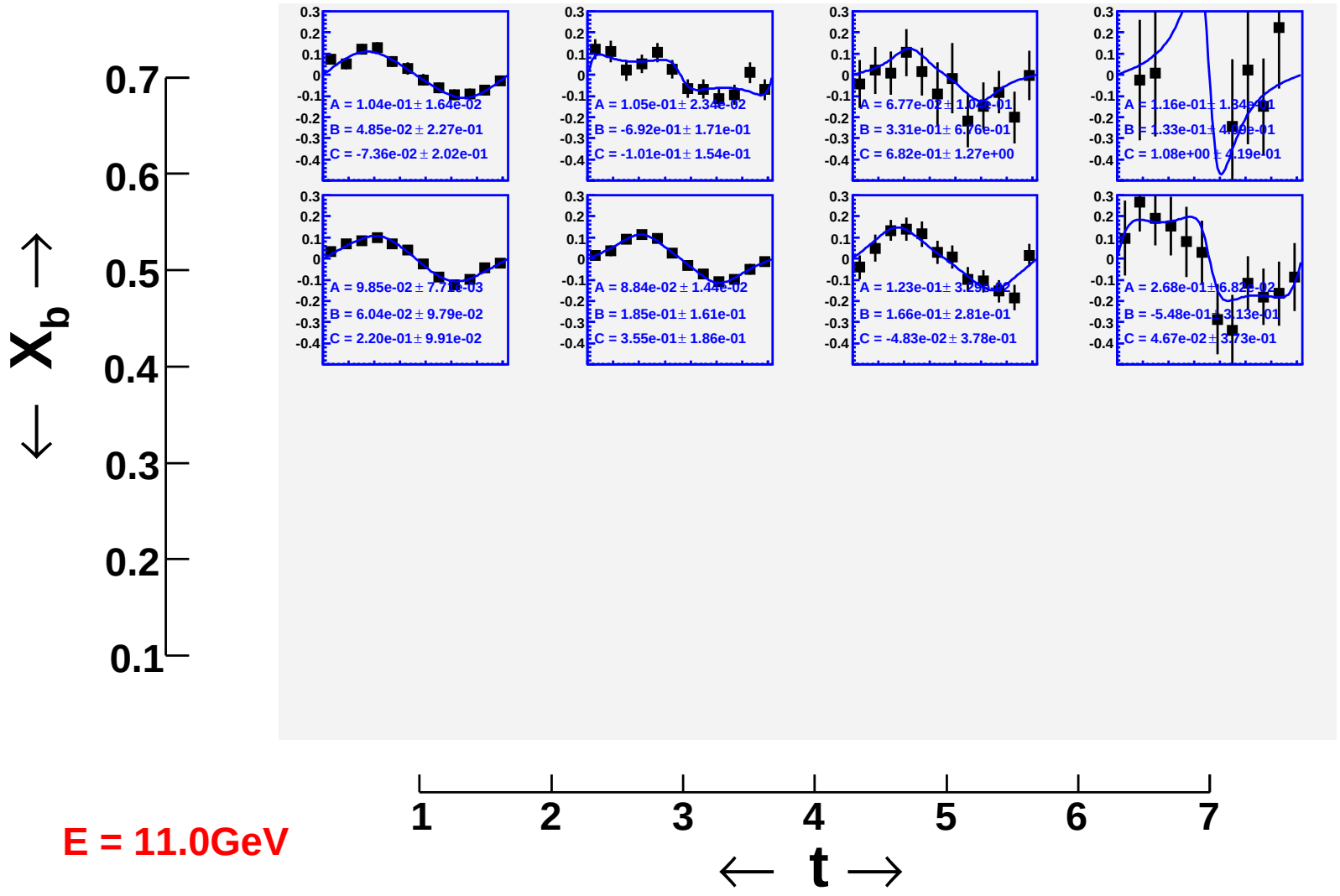

FIG. 25: Simulated $A\sin\phi/(1+B\cos 2\phi + C\cos\phi)$ asymmetries for the reaction $ep \to ep\pi^0$, $\pi^0 \to \gamma\gamma$ at $Q^2 = 8\ GeV^2$.

CLAS12 acceptance of ϵ vs. Q^2 at 6.6, 8.8 and 11 GeV incident beams at $< x_B >= 0.35$ and $\Delta x_B = 0.1$. The procedure to extract σ_T and σ_L is then to apply a straight line to extracted $\sigma_T + \epsilon\sigma_L$ values for different ϵ points at each fixed Q^2, x_B and t point. The intercept at ϵ=0 yields σ_T, and the slope gives σ_L.

Table I shows estimated number of events at $< x_B >$=0.35 for different Q^2 and t bins based on 2000 hours running time for beam energy 11.0 GeV and 500 hours running time each for beam energies 8.8 and 6.6 GeV. The bin sizes are ΔQ^2=0.5 GeV^2, Δx_B=0.1 and Δt=1.0 GeV^2. Table I clearly shows that the proposed experiment covers from low to high Q^2 and low to high t with reasonable statistics and reasonable size of ϵ lever arm. Table II shows estimated number of events at low t ($t < 1$) bins $< x_B >$=0.35 for different Q^2 and t bins based on 2000 hours running time for beam energy 11.0 GeV and 500 hours running time each for beam energies 8.8 and 6.6 GeV. The bin sizes are ΔQ^2=0.5 GeV^2, Δx_B=0.1 and Δt=0.1 GeV^2.

D. Estimated Systematic Errors

Since the CLAS12 detector is still in the design stage, it is not possible to perform detailed analysis on systematic errors. However, the general goals of the detector design are understood and are used to estimate systematics for the proposed measurements. Systematic error source and its estimation are itemized in the Table III. The systematic error for separated structure functions (σ_L, σ_T) is magnified by $1/\Delta\epsilon$.

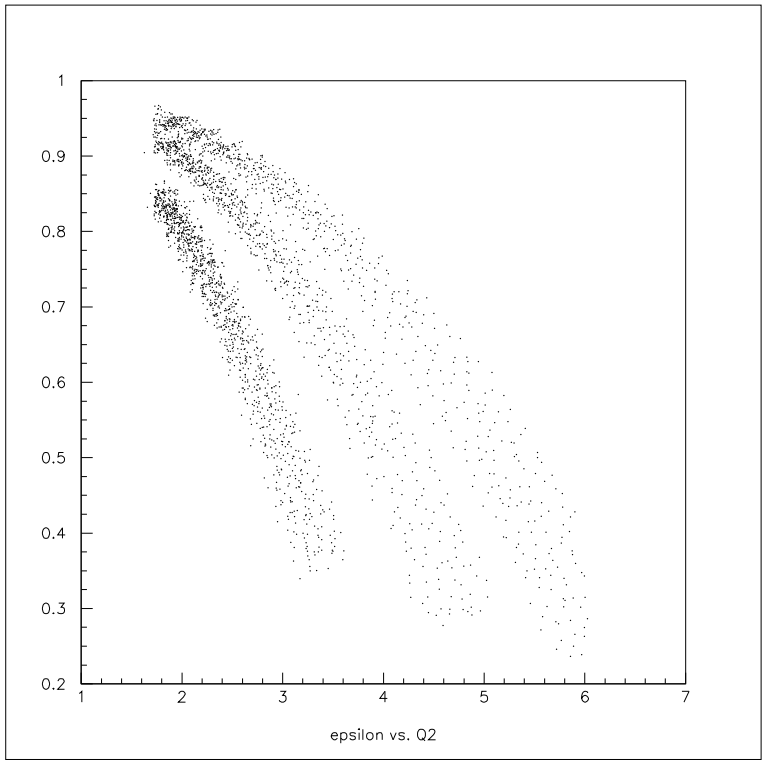

FIG. 26: The CLAS12 acceptance of ϵ vs. Q^2 at 6.6, 8.8 and 11 GeV incident beams at $< x_B >=$ 0.35 and $\Delta x_B = 0.1$

TABLE I: Estimated number of events at $< x_B >$=0.35 for different Q^2 and t bins based on 2000 hours running time for beam energy 11.0 GeV and 500 hours running time each for beam energies 8.8 and 6.6 GeV. The bin sizes are ΔQ^2=0.5 GeV^2, Δx_B=0.1 and Δt=1.0 GeV^2, except for the bin at $-t = 6.5$ where Δt=2.0 GeV^2

.

Q^2	ϵ	$< -t >$ (GeV^2)							E_b
GeV^2		0.5	1.5	2.5	3.5	4.5	5.5	6.5	GeV
5.0	0.533	0.59e5	0.30e5	0.11e5	0.44e4	0.19e4	0.76e3	0.30e3	11.0
	0.266	0.13e5	0.73e4	0.30e4	0.12e4	0.46e3	0.18e3	0.87e2	8.8
4.5	0.634	0.89e5	0.43e5	0.16e5	0.62e4	0.26e4	0.11e4	0.37e3	11.0
	0.384	0.86e5	0.47e5	0.18e5	0.76e4	0.32e4	0.12e4	0.43e3	8.8
4.0	0.721	0.14e6	0.62e5	0.24e5	0.89e4	0.36e4	0.13e4	0.39e3	11.0
	0.526	0.15e6	0.79e5	0.30e5	0.12e5	0.48e4	0.17e4	0.51e3	8.8
3.5	0.794	0.22e6	0.95e5	0.36e5	0.12e5	0.40e4	0.13e4	0.36e3	11.0
	0.650	0.25e6	0.12e6	0.45e5	0.16e5	0.62e5	0.17e4	0.42e3	8.8
	0.320	0.94e5	0.51e5	0.20e5	0.84e4	0.29e4	0.69e3	0.98e2	6.6
3.0	0.854	0.37e6	0.15e6	0.50e5	0.13e5	0.40e4	0.13e4	0.14e3	11.0
	0.754	0.43e6	0.20e6	0.68e5	0.68e5	0.19e5	0.15e4	0.17e3	8.8
	0.515	0.48e6	0.25e6	0.90e5	0.33e5	0.96e4	0.19e4	0.15e3	6.6
2.5	0.902	0.62e6	0.24e6	0.57e6	0.11e5	0.33e4	0.43e3	0.00e0	11.0
	0.836	0.77e6	0.33e6	0.81e5	0.16e5	0.54e4	0.46e3	0.00e0	8.8
	0.677	0.91e6	0.44e6	0.12e6	0.31e5	0.74e4	0.47e3	0.00e0	6.6
2.0	0.939	0.96e6	0.29e6	0.56e5	0.56e4	0.91e3	0.00e0	0.00e0	11.0
	0.899	0.13e7	0.43e6	0.80e5	0.97e4	0.14e4	0.00e0	0.00e0	8.8
	0.803	0.17e7	0.62e6	0.12e6	0.21e5	0.16e4	0.00e0	0.00e0	6.6

TABLE II: Estimated number of events at $< x_B >$=0.35 for different Q^2 and low t bins ($t < 1.0$) based on 2000 hours running time for beam energy 11.0 GeV and 500 hours running time each for beam energies 8.8 and 6.6 GeV. The bin sizes are ΔQ^2=0.5 GeV^2, Δx_B=0.1 and Δt=0.1 GeV^2.

Q^2	ϵ	$< -t >$ GeV^2									E$_b$
GeV^2		0.15	0.25	0.35	0.45	0.55	0.65	0.75	0.85	0.95	GeV
5.0	0.533	0.38e4	0.10e5	0.87e4	0.75e4	0.64e4	0.59e4	0.53e4	0.45e4	0.35e4	11.0
5.0	0.266	0.42e3	0.17e4	0.17e4	0.17e4	0.16e4	0.16e4	0.14e4	0.12e4	0.88e3	8.8
4.5	0.634	0.38e4	0.10e5	0.87e4	0.75e4	0.64e4	0.59e4	0.53e4	0.45e4	0.35e4	11.0
4.5	0.634	0.46e4	0.13e5	0.12e5	0.11e5	0.11e5	0.98e4	0.87e4	0.72e4	0.56e4	8.8
4.0	0.721	0.12e5	0.27e5	0.22e5	0.19e5	0.15e5	0.13e5	0.11e5	0.91e4	0.71e4	11.0
4.0	0.526	0.10e5	0.25e5	0.21e5	0.19e5	0.17e5	0.15e5	0.14e5	0.12e5	0.94e4	8.8
3.5	0.794	0.20e5	0.44e5	0.37e5	0.30e5	0.24e5	0.20e5	0.17e5	0.14e5	0.11e5	11.0
3.5	0.526	0.20e5	0.45e5	0.37e5	0.31e5	0.27e5	0.24e5	0.21e5	0.18e5	0.14e5	8.8
3.0	0.854	0.34e5	0.72e5	0.61e5	0.49e5	0.40e5	0.33e5	0.28e5	0.23e5	0.18e5	11.0
3.0	0.754	0.38e5	0.79e5	0.66e5	0.54e5	0.46e5	0.40e5	0.35e5	0.30e5	0.23e5	8.8
3.0	0.515	0.34e5	0.74e5	0.66e5	0.59e5	0.55e5	0.51e5	0.46e5	0.40e5	0.30e5	6.6
2.5	0.902	0.59e5	0.12e6	0.10e6	0.81e5	0.66e5	0.55e5	0.46e5	0.38e5	0.29e5	11.0
2.5	0.836	0.71e5	0.15e6	0.12e6	0.98e5	0.82e5	0.70e5	0.61e5	0.52e5	0.40e5	8.8
2.5	0.677	0.76e5	0.15e6	0.13e6	0.11e6	0.10e6	0.91e5	0.83e5	0.71e5	0.55e5	6.6
2.0	0.939	0.10e6	0.20e6	0.16e6	0.13e6	0.10e6	0.81e5	0.66e5	0.53e5	0.37e5	11.0
2.0	0.899	0.13e6	0.26e6	0.21e6	0.17e6	0.14e6	0.12e6	0.10e6	0.82e5	0.59e5	8.8
2.0	0.803	0.16e5	0.30e6	0.25e6	0.21e6	0.19e6	0.17e5	0.15e6	0.12e6	0.92e5	6.6

TABLE III: Anticipated systematic errors based on our previous experience from the CLAS experiment analysis at 6 GeV, and the CLAS12 design parameters. $\sigma_U = \sigma_T + \epsilon\sigma_L$.

Source	Error Estimation
Acceptance	2.5 %
Target Thickness	0.2 %
Beam Charge	0.2 %
PID	1.0 %
Monte Carlo Generator	0.5 %
Radiative Corrections	1.0 %
σ_U,σ_{TT}, σ_{LT},$\sigma_{LT'}$	2.9 %
σ_L, σ_T	9.0 %

VI. BEAM TIME ESTIMATES AND RUNNING CONDITIONS

The 11 GeV data taking will use the same running conditions as the DVCS experiment, and the two will run contemporaneously on CLAS12. The beam time request for the 11 GeV part of the proposal is 2000 hrs.

The requested beam time for the 8.8 and 6.6 GeV running is 500 hrs each. These lower energies are required for Rosenbluth L/T separation. We expect these will run during the periods when Hall-B is required to receive less than 11 GeV beam. We are hopeful that in the years leading up to the upgrade improvements in analysis techniques and more precise calibrations compared with those presently used may further shorten the lower energy beam time requirements.

VII. CONCLUSIONS

The proposed experiment on π^0 and η production forms an integral and essential part of the CLAS12 program of exclusive electroproduction measurements aimed at exploring the quark structure of the nucleon. The planned measurements in the high–Q^2, low–t region will allow us to test the approach to the partonic reaction mechanism in unprecedented detail, and will provide unique information about the spatial distribution of quark spin (polarized GPDs) in the nucleon. The measurements in the high–t region will for the first time explore the region of both high–t and high–Q^2, where meson production is predicted to be dominated by a partonic mechanism. Experience with measurements at lower beam energies and the Monte–Carlo based projections to the JLab upgrade energies show that the planned experiment is feasible, and that the statistics will be reasonable even at the highest Q^2 and t values envisaged. In view of the current developments in theory we expect significant impulses for the analysis of the forthcoming data and their interpretation in terms of GPDs as the experimental preparations progress.

[1] A. V. Radyushkin, Phys. Lett. B **380**, 417 (1996) [arXiv:hep-ph/9604317].

[2] X. D. Ji, Phys. Rev. D **55**, 7114 (1997) [arXiv:hep-ph/9609381].

[3] J. C. Collins, L. Frankfurt and M. Strikman, Phys. Rev. D **56**, 2982 (1997) [arXiv:hep-ph/9611433].

[4] D. Mueller, D. Robaschik, B. Geyer, F. M. Dittes and J. Horejsi, Fortsch. Phys. **42**, 101 (1994) [arXiv:hep-ph/9812448].

[5] A. V. Radyushkin, Phys. Rev. D **56**, 5524 (1997) [arXiv:hep-ph/9704207].

[6] A. V. Radyushkin, Phys. Rev. D **58**, 114008 (1998) [arXiv:hep-ph/9803316].

[7] M. Diehl, T. Feldmann, R. Jakob and P. Kroll, Eur. Phys. J. C **8**, 409 (1999) [arXiv:hep-ph/9811253].

[8] H. W. Huang and P. Kroll, Eur. Phys. J. C **17**, 423 (2000) [arXiv:hep-ph/0005318].

[9] L. Mankiewicz, G. Piller and A. Radyushkin, Eur. Phys. J. C **10**, 307 (1999) [arXiv:hep-ph/9812467].

[10] L. L. Frankfurt, P. V. Pobylitsa, M. V. Polyakov and M. Strikman, Phys. Rev. D **60**, 014010 (1999) [arXiv:hep-ph/9901429].

[11] K. Goeke, M. V. Polyakov and M. Vanderhaeghen, Prog. Part. Nucl. Phys. **47**, 401 (2001) [arXiv:hep-ph/0106012].

[12] R. Jakob, P. Kroll and M. Raulfs, J. Phys. G **22**, 45 (1996) [arXiv:hep-ph/9410304]; P. Kroll and M. Raulfs, Phys. Lett. B **387**, 848 (1996) [arXiv:hep-ph/9605264].

[13] I. V. Musatov and A. V. Radyushkin, Phys. Rev. D **56**, 2713 (1997) [arXiv:hep-ph/9702443].

[14] J. Gronberg *et al.* [CLEO Collaboration], Phys. Rev. D **57**, 33 (1998) [arXiv:hep-ex/9707031].

[15] A. C. Irving and R. P. Worden, Phys. Rept. **34**, 117 (1977).

[16] J. K. Storrow, Rept. Prog. Phys. **50**, 1229 (1987).

[17] F. W. Brasse *et al.*, Phys. Lett. B **58**, 467 (1975).

[18] C. Berger *et al.*, Nucl. Phys. B **137**, 1 (1978).

[19] P. D. B. Collins and T. D. B. Wilkie, Z. Phys. C **7**, 357 (1981).

[20] M. Diehl, Phys. Rept. **388**, 41 (2003) [arXiv:hep-ph/0307382].

[21] A. V. Belitsky and A. V. Radyushkin, Phys. Rept. **418**, 1 (2005) [arXiv:hep-ph/0504030].

[22] M. Burkardt, Int. J. Mod. Phys. A **18**, 173 (2003) [arXiv:hep-ph/0207047].

[23] M. Diehl, Eur. Phys. J. C **25**, 223 (2002) [Erratum-ibid. C **31**, 277 (2003)] [arXiv:hep-ph/0205208].

[24] A. Levy, Nucl. Phys. Proc. Suppl. **146**, 92 (2005).

[25] L. Frankfurt, M. Strikman and C. Weiss, Ann. Rev. Nucl. Part. Sci. **55**, 403 (2005) [arXiv:hep-ph/0507286].

[26] M. Guidal, J. M. Laget and M. Vanderhaeghen, Nucl. Phys. A **627**, 645 (1997).

[27] H. Harari, Phys. Rev. Lett. **27**, 1028 (1971).

[28] M. I. Eides, L. L. Frankfurt and M. I. Strikman, Phys. Rev. D **59**, 114025 (1999) [arXiv:hep-ph/9809277].

[29] M. Diehl, W. Kugler, A. Schafer and C. Weiss, Phys. Rev. D **72**, 034034 (2005) [Erratum-ibid. D **72**, 059902 (2005)] [arXiv:hep-ph/0506171].

[30] T. H. Bauer, R. D. Spital, D. R. Yennie and F. M. Pipkin, Rev. Mod. Phys. **50**, 261 (1978) [Erratum-ibid. **51**, 407 (1979)].

[31] L. Frankfurt, W. Koepf and M. Strikman, Phys. Rev. D **54**, 3194 (1996) [arXiv:hep-ph/9509311].

[32] M. Penttinen, M. V. Polyakov and K. Goeke, Phys. Rev. D **62**, 014024 (2000) [arXiv:hep-ph/9909489].

[33] J. Volmer *et al.* [The Jefferson Lab F(pi) Collaboration], Phys. Rev. Lett. **86**, 1713 (2001) [arXiv:nucl-ex/0010009].

[34] M. Diehl, T. Feldmann, R. Jakob and P. Kroll, "Generalized parton distributions from nucleon form factor data," Eur. Phys. J. C **39**, 1 (2005) [arXiv:hep-ph/0408173].

[35] T. C. Brooks and L. J. Dixon, Phys. Rev. D **62**, 114021 (2000) [arXiv:hep-ph/0004143].

[36] D. J. Hamilton *et al.* [Jefferson Lab Hall A Collaboration], Phys. Rev. Lett. **94**, 242001 (2005) [arXiv:nucl-ex/0410001].

[37] H. W. Huang, R. Jakob, P. Kroll and K. Passek-Kumericki, Eur. Phys. J. C **33**, 91 (2004) [arXiv:hep-ph/0309071].

[38] C. Hadjidakis *et al.* [CLAS Collaboration], "Exclusive rho0 meson electroproduction from hydrogen at CLAS," Phys. Lett. B **605**, 256 (2005) [arXiv:hep-ex/0408005].

[39] L. Morand *et al.* [CLAS Collaboration], "Deeply virtual and exclusive electroproduction of omega mesons," Eur. Phys. J. A **24**, 445 (2005) [arXiv:hep-ex/0504057].

[40] V. Kubarovsky, "Deeply Virtual Meson Electroproduction", presented at: The Next Seven

Years: International Workshop on the Jlab Near Term Physics Program, Newport News, Va, June 16-18, 2004.

[41] R. Niyazov, http://www1.jlab.org/ul/Physics/Hall-B/clas/public/2005-021.ps

[42] F.–X. Girod, http://www1.jlab.org/ul/Physics/Hall-B/clas/public/2005-001.ps

APPENDIX A: FURTHER INFORMATION ON CLAS12 SIMULATIONS

In this appendix we provide further details on the simulations for the proposed experiment. The CLAS12 acceptances and projected data for the $ep \rightarrow e'p\gamma\gamma$ reaction was estimated via Monte-Carlo simulations. For the purposes of rate estimates, events were generated assuming an experimental run of 1000 hours, which is several times smaller than we would expect in an extended run involving several proposed experiments. The kinematic landscape for accepted events and the numerical distributions for each variable integrated over the other variables have been shown in Figs. 18 and 19. Note that the expected rates are quite substantial even at the higher values of Q^2 and $-t$.

Figures 28, 29, 30, show various distributions which are of typical interest in analysis of an experiment of this type.

Figures 31 and 32, show the CLAS12 acceptance as a function of x_B, Q^2, W, and t for the reactions $ep \rightarrow ep\pi^0$ ($\pi^0 \rightarrow \gamma\gamma$), and $ep \rightarrow ep\eta$ ($\eta \rightarrow \gamma\gamma$) respectively. Note that the π^0 and η acceptances are similar each other.

Figures 33, 34, 35, and 36 present the CLAS12 statistics of accepted events as a function of t and Q^2, for different W, Q^2, and t bins for the reactions $ep \rightarrow ep\pi^0$, $\pi^0 \rightarrow \gamma\gamma$ when both photons are detected in the calorimeters.

Figures 37, 38, 39, and 40 present the CLAS12 statistics of accepted events as a function of t and Q^2, for different W, Q^2, and t bins for the reactions $ep \rightarrow ep\eta$, $\eta \rightarrow \gamma\gamma$ when both photons are detected in the calorimeters.

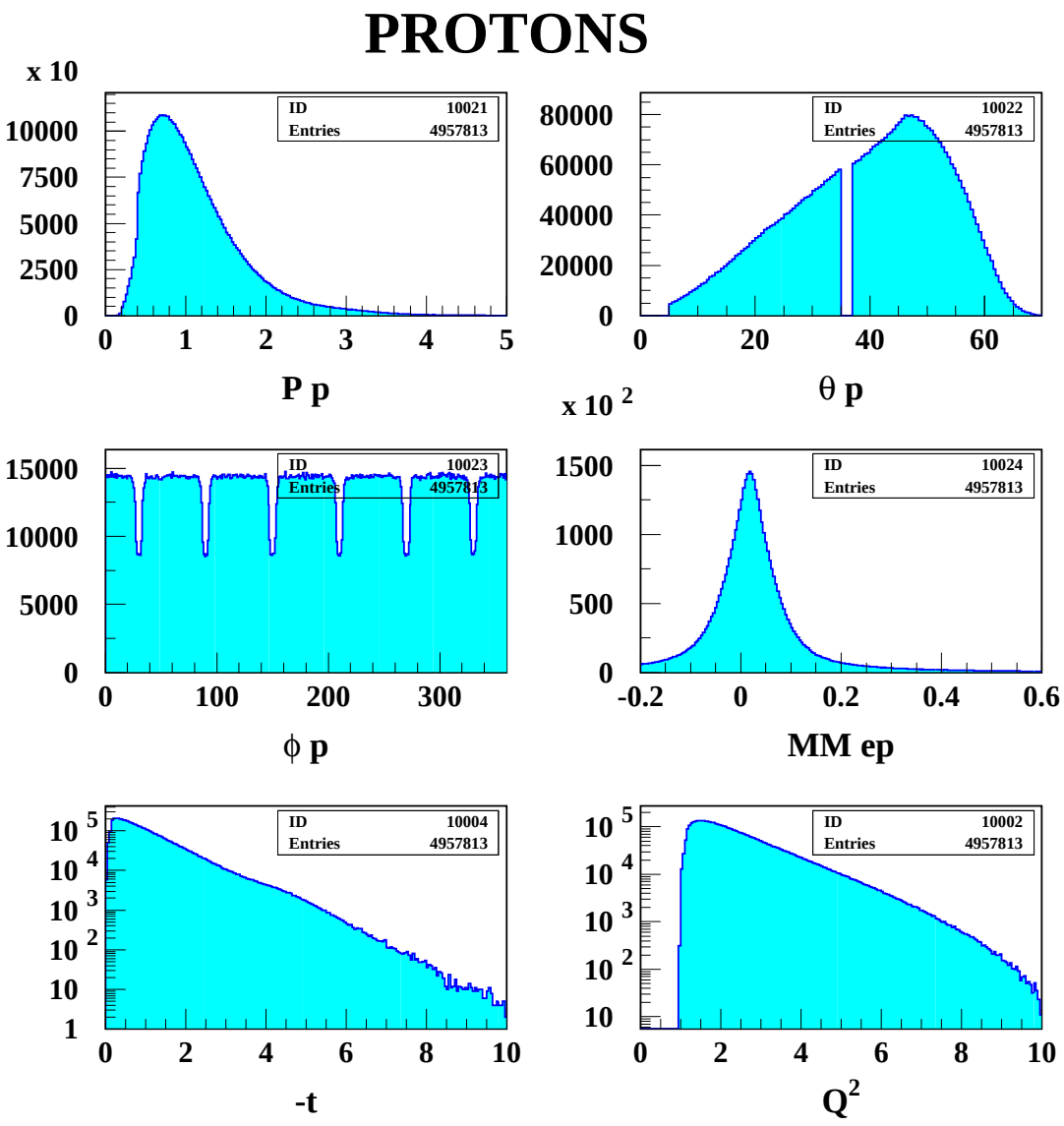

FIG. 27: Reaction $ep \to ep\pi^0$. Monte Carlo simulation. The momentum, angular(θ and ϕ), t, and Q^2 distribution for protons.

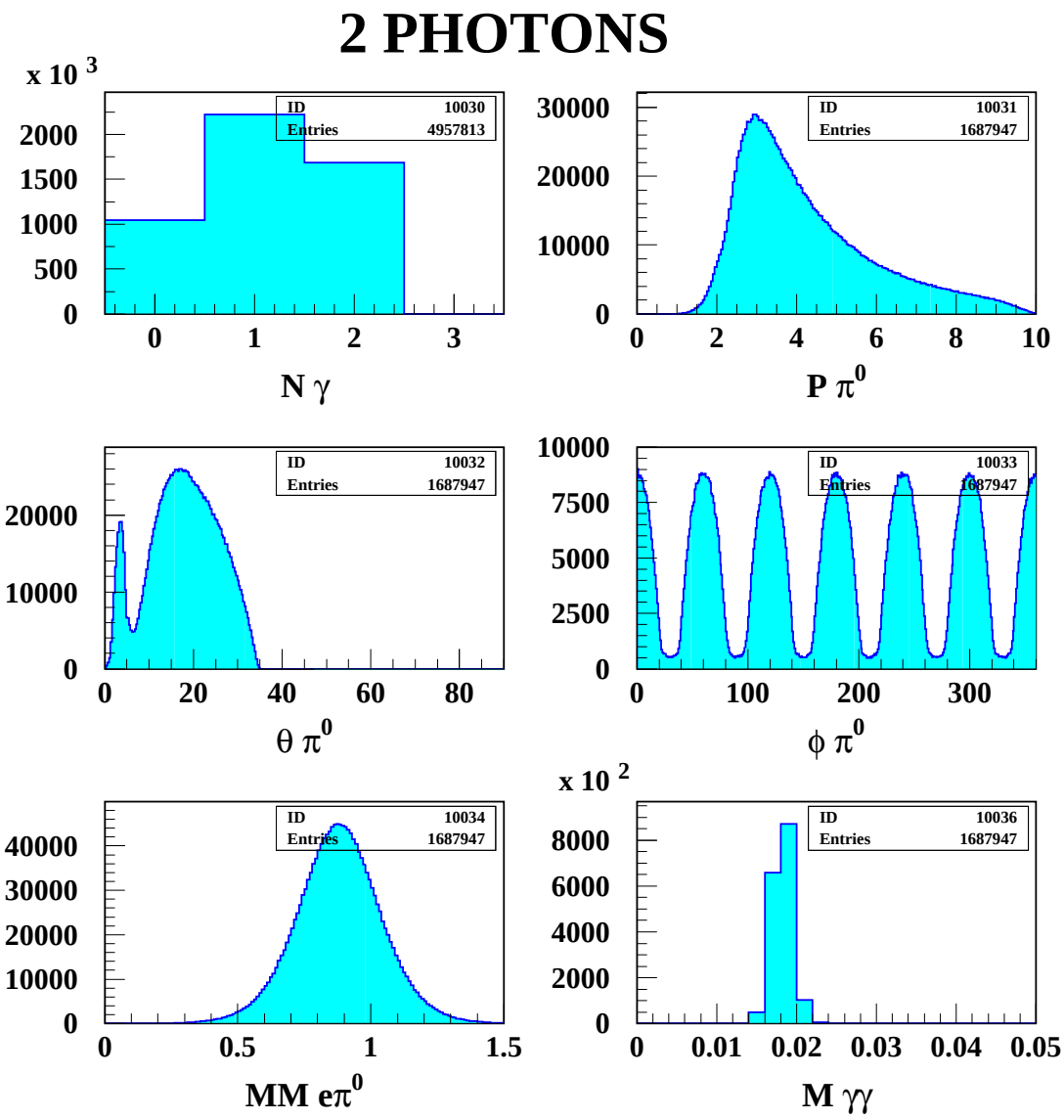

FIG. 28: Reaction $ep \to ep\pi^0$, $\pi^0 \to \gamma\gamma$. Monte Carlo simulation. Top left: the multiplicity of the accepted by the calorimeters photons. The momentum, angular(θ and ϕ), missing mass to $e\pi^0$, and invarint mass $M_{\gamma\gamma}$ distributions for photons, when both photons are accepted.

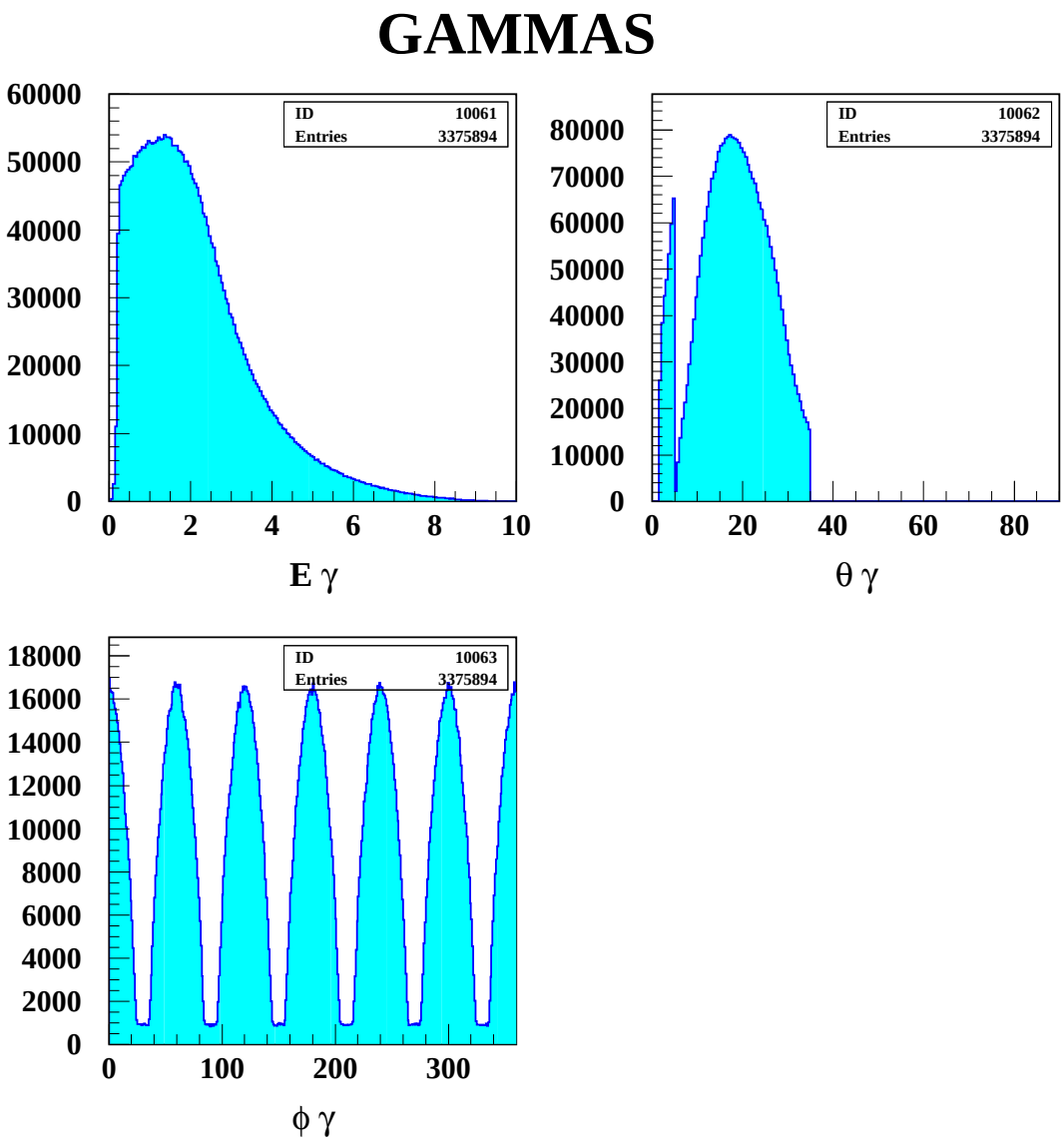

FIG. 29: The energy and angular(θ and ϕ) distributions for photons.

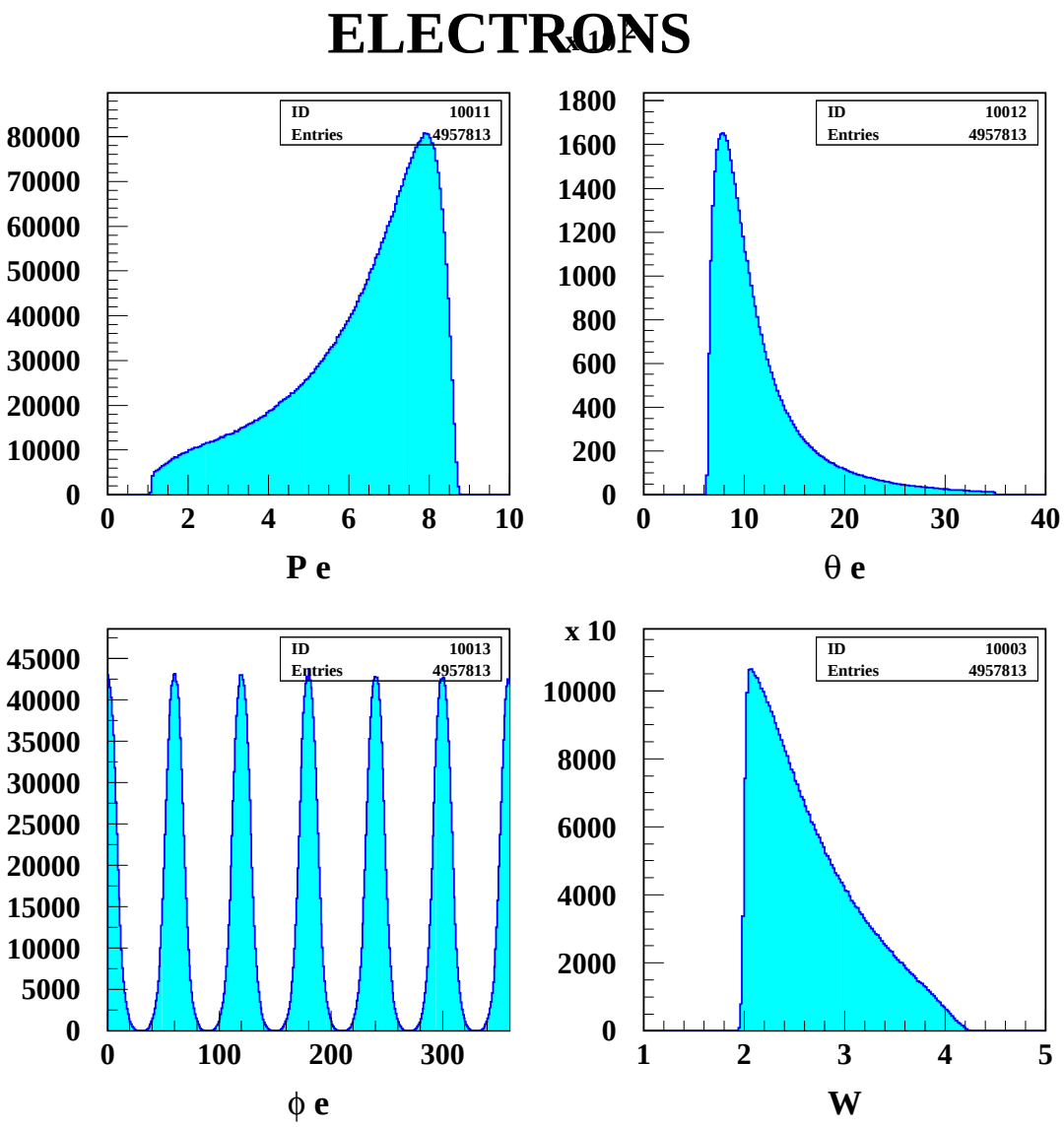

FIG. 30: The momentum, angular (θ and ϕ) distributions for electrons.

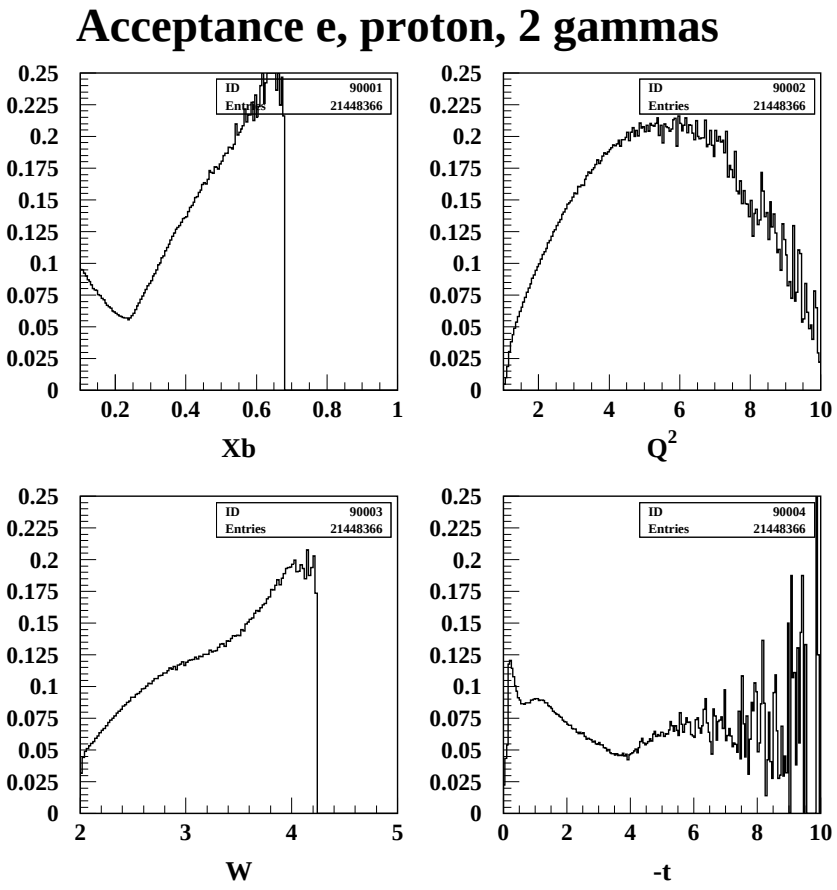

FIG. 31: Reaction $ep \to ep\pi^0$, $\pi^0 \to \gamma\gamma$. The CLAS12 acceptance as a function of x_B, Q^2, W, and t for the events with electron, proton and two gammas are detected.

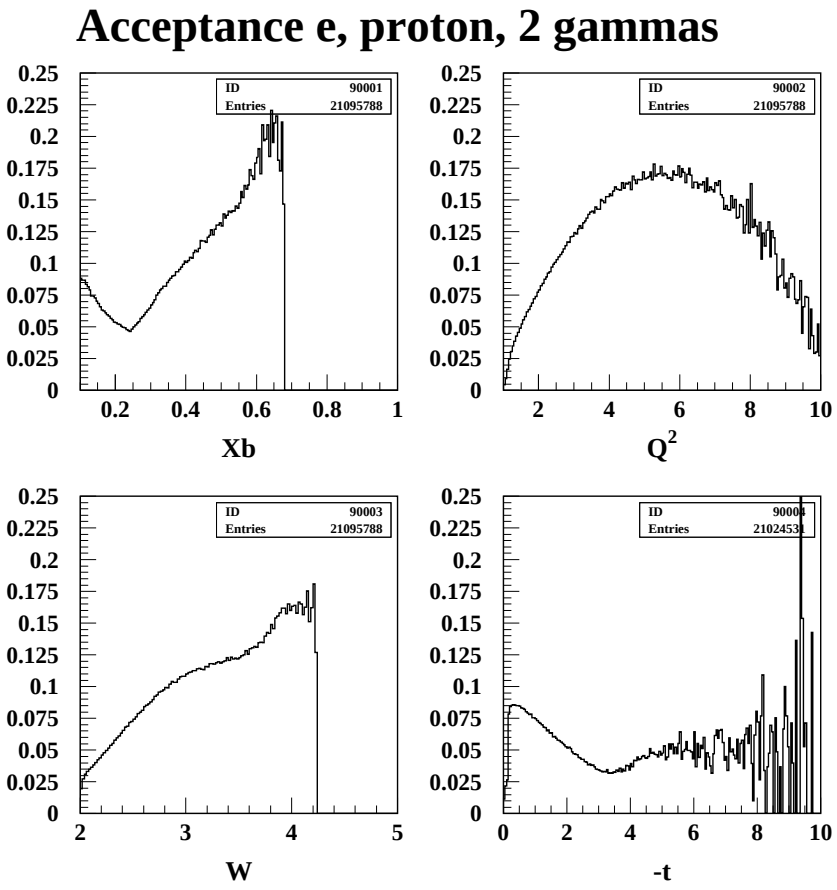

FIG. 32: Reaction $ep \to ep\eta$, $\eta \to \gamma\gamma$. The CLAS12 acceptance as a function of x_B, Q^2, W, and t for the events with electron, proton and two gammas are detected.

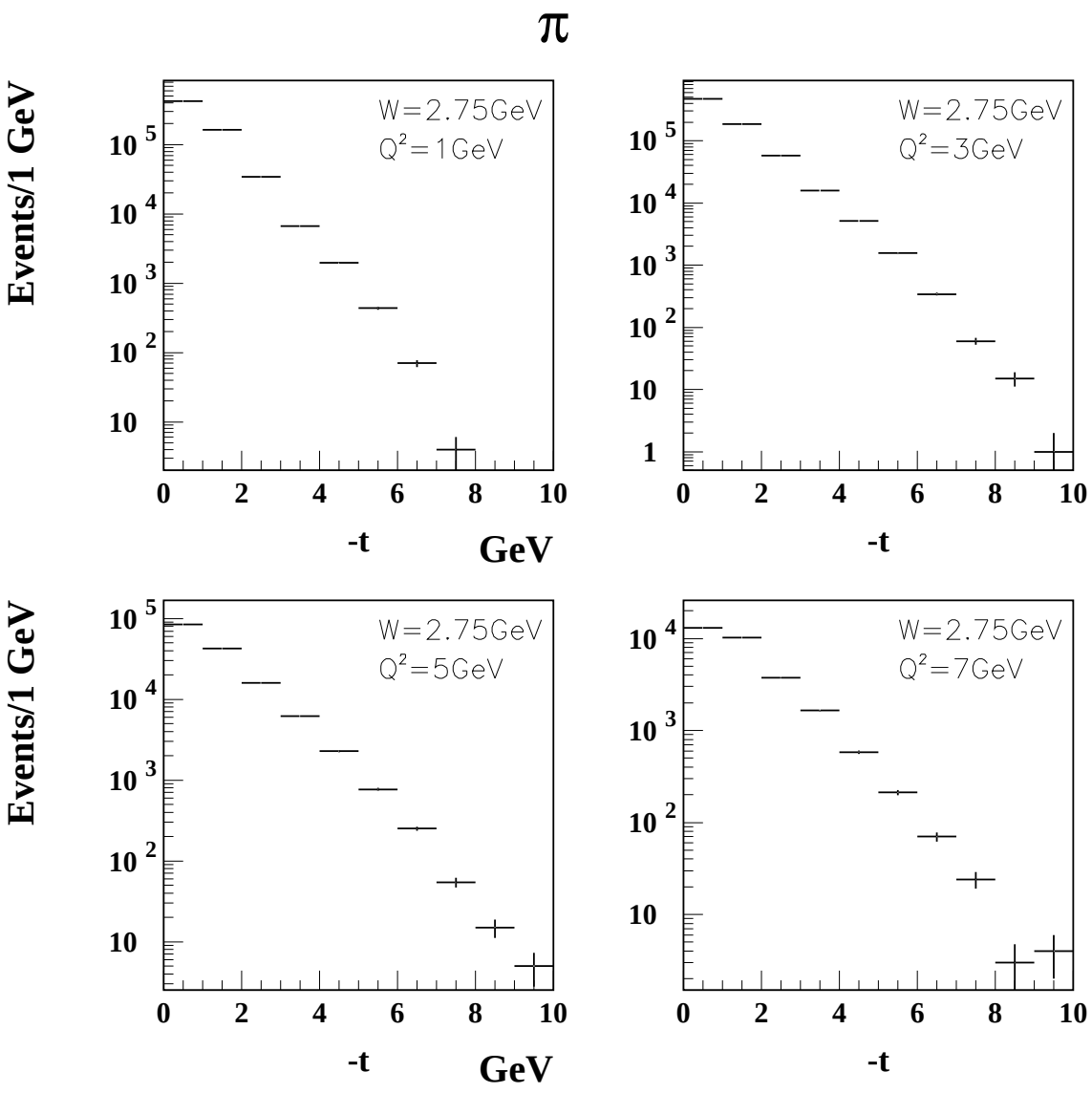

FIG. 33: Reaction $ep \to ep\pi^0$, $\pi^0 \to \gamma\gamma$. t distribution for $W = 2.75 \pm 0.75$ GeV and different Q^2 bins with $\Delta Q^2 = 2$ Gev^2. Statistics corresponds to 1000 hours of the CLAS12 operation.

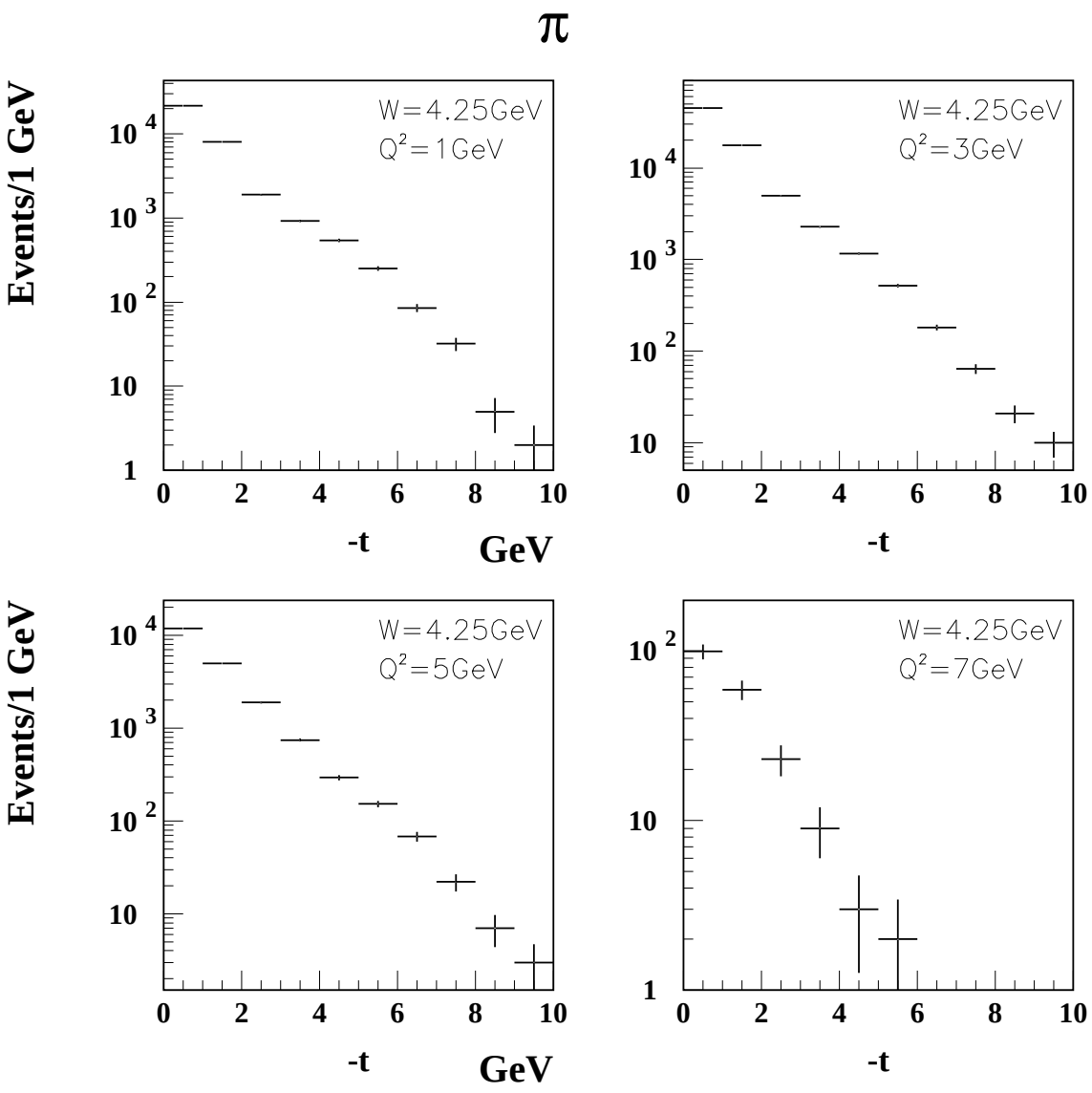

FIG. 34: Reaction $ep \to ep\pi^0$, $\pi^0 \to \gamma\gamma$. t distribution for $W = 4.25 \pm 0.75$ GeV and different Q^2 bins with $\Delta Q^2 = 2$ Gev^2. Statistics corresponds to 1000 hours of the CLAS12 operation.

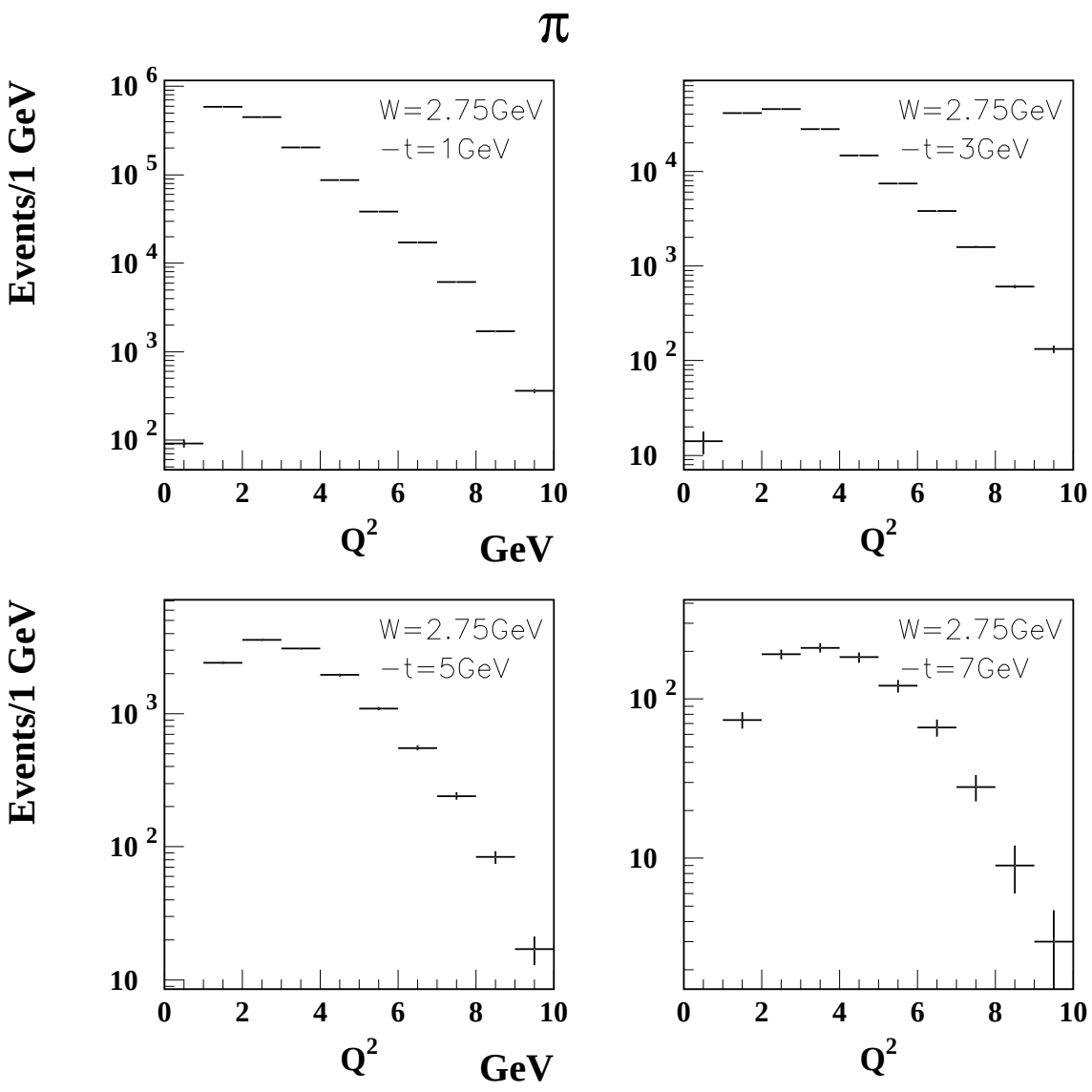

FIG. 35: Reaction $ep \to ep\pi^0$, $\pi^0 \to \gamma\gamma$. Q^2 distribution for $W = 2.75 \pm 0.75$ and different t bins with $\Delta t = 2$ Gev^2. Statistics corresponds to 1000 hours of the CLAS12 operation.

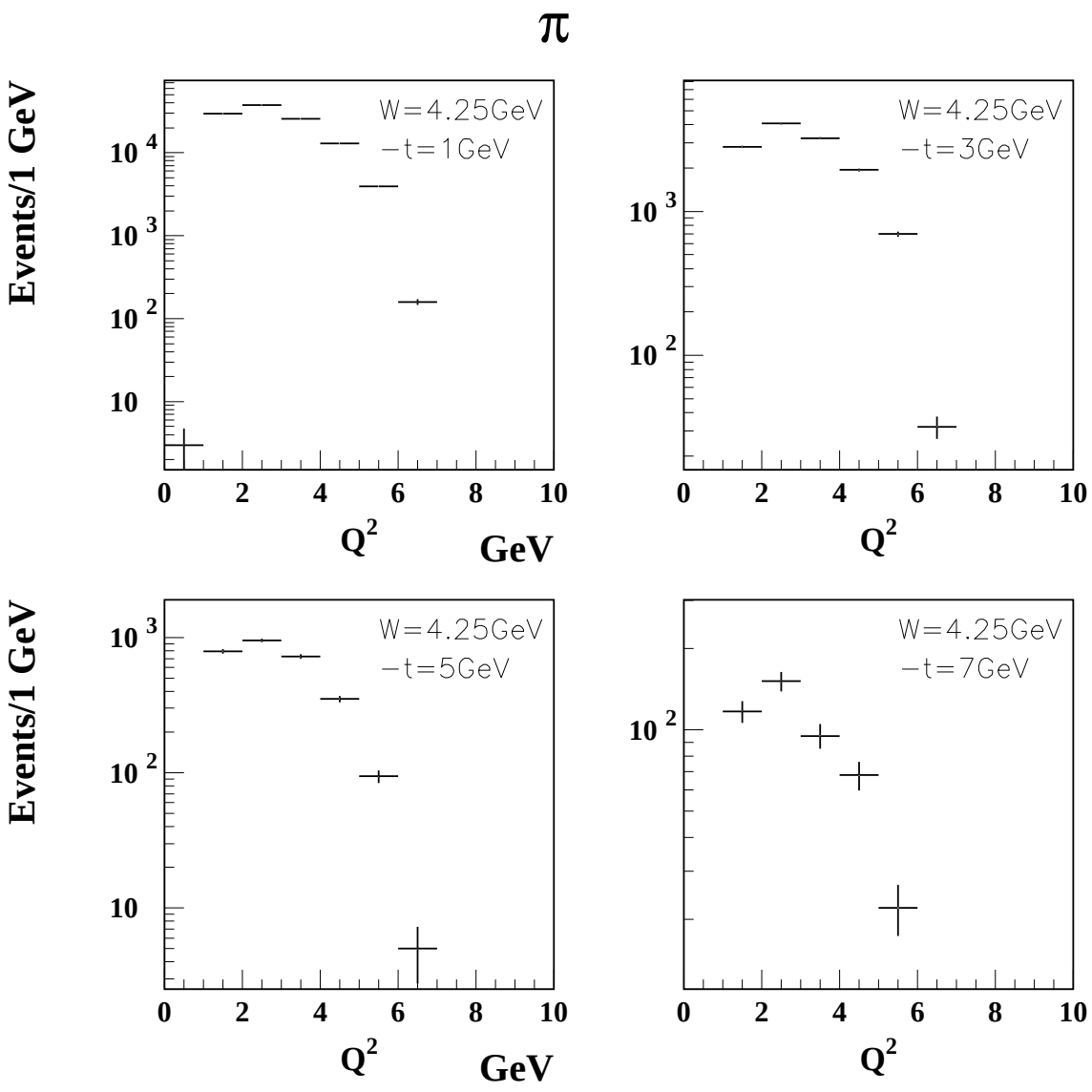

FIG. 36: Reaction $ep \to ep\pi^0$, $\pi^0 \to \gamma\gamma$. Q^2 distribution for $W = 4.25 \pm 0.75$ and different t bins with $\Delta t = 2$ Gev^2. Statistics corresponds to 1000 hours of the CLAS12 operation.

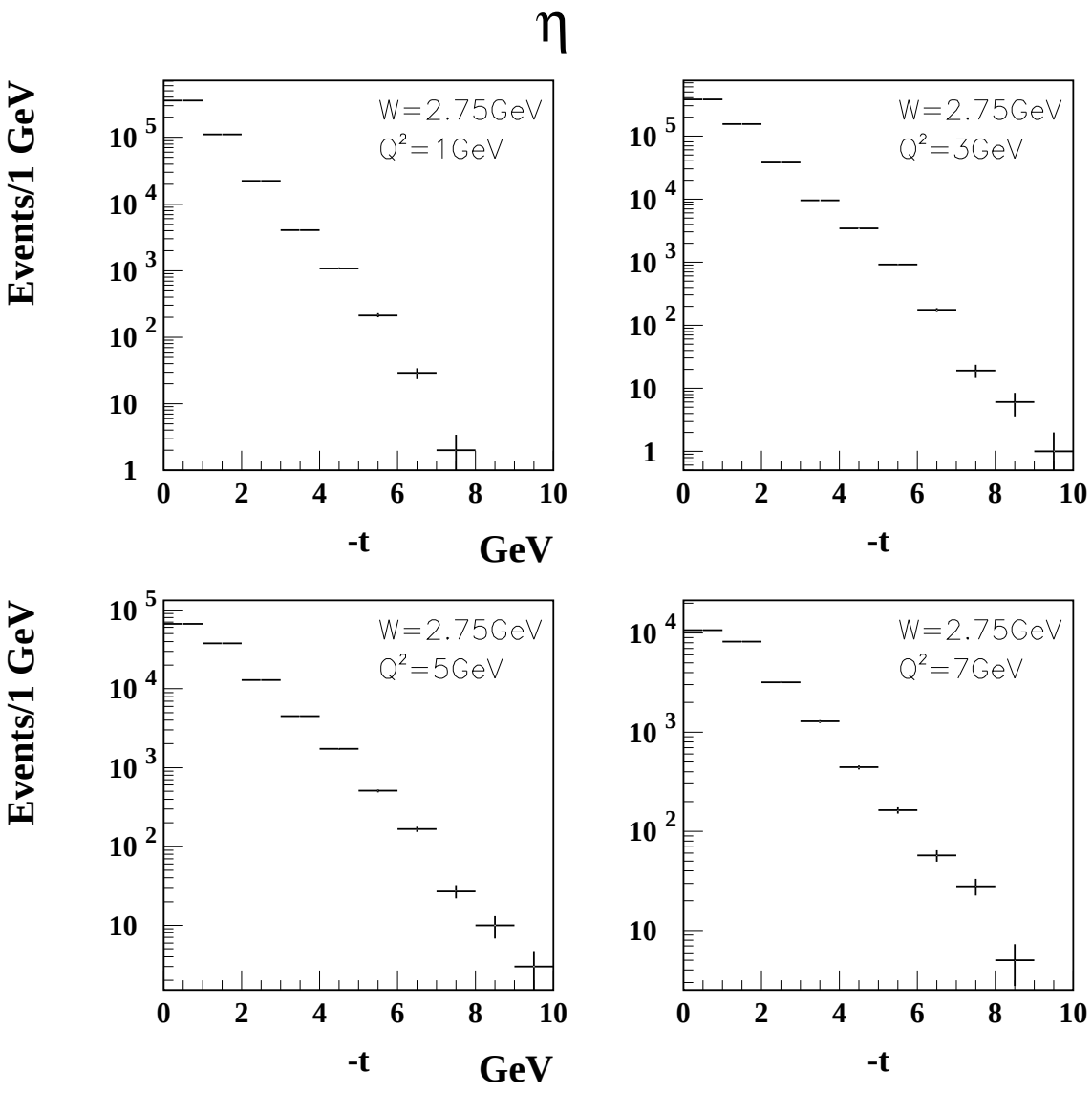

FIG. 37: Reaction $ep \to ep\eta$, $\eta \to \gamma\gamma$. t distribution for $W = 2.75 \pm 0.75$ GeV and different Q^2 bins with $\Delta Q^2 = 2$ Gev^2. Statistics corresponds to 1000 hours of the CLAS12 operation.

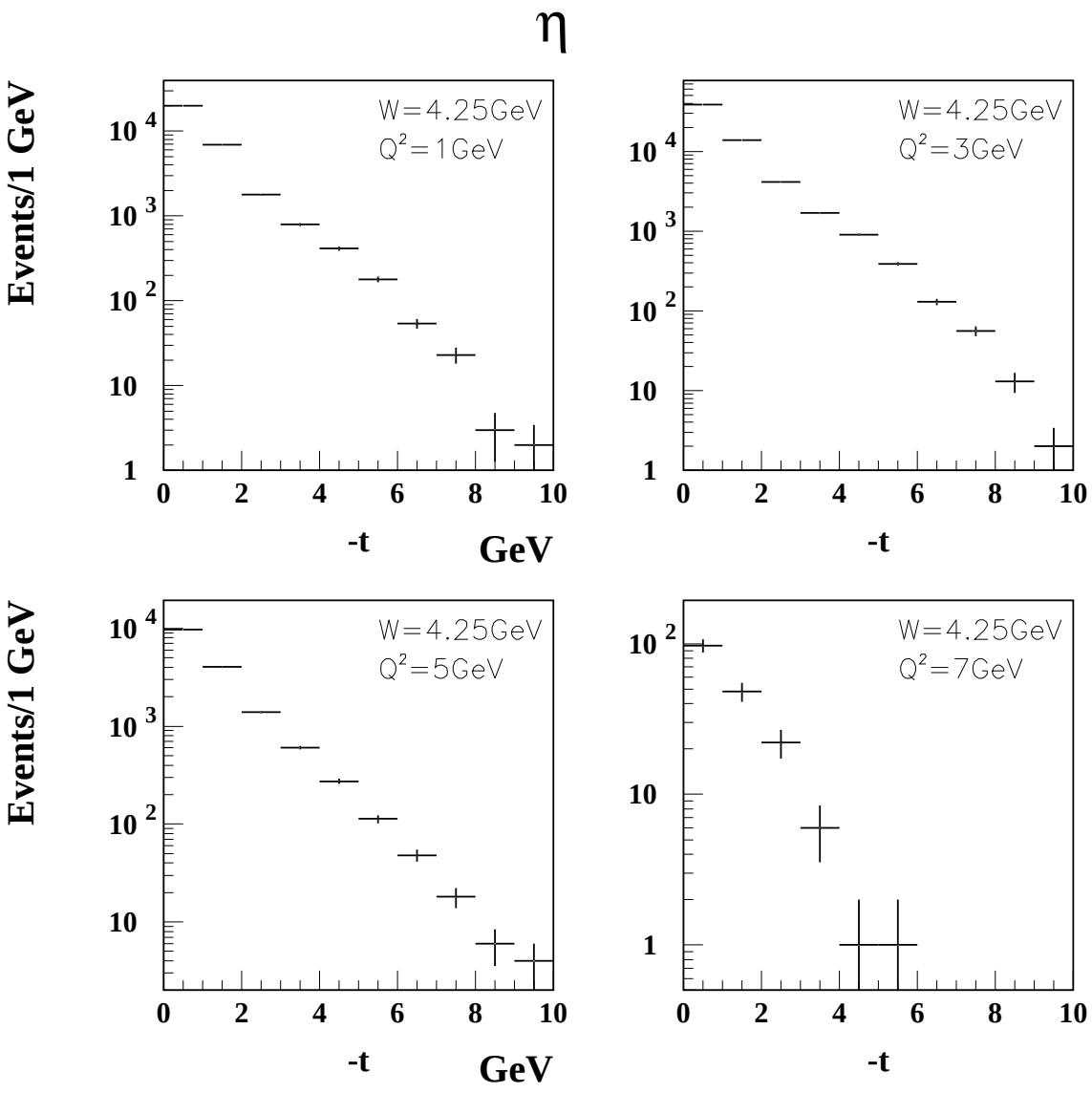

FIG. 38: Reaction $ep \to ep\eta$, $\eta \to \gamma\gamma$. t distribution for $W = 4.25 \pm 0.75$ GeV and different Q^2 bins with $\Delta Q^2 = 2$ Gev^2. Statistics corresponds to 1000 hours of the CLAS12 operation.

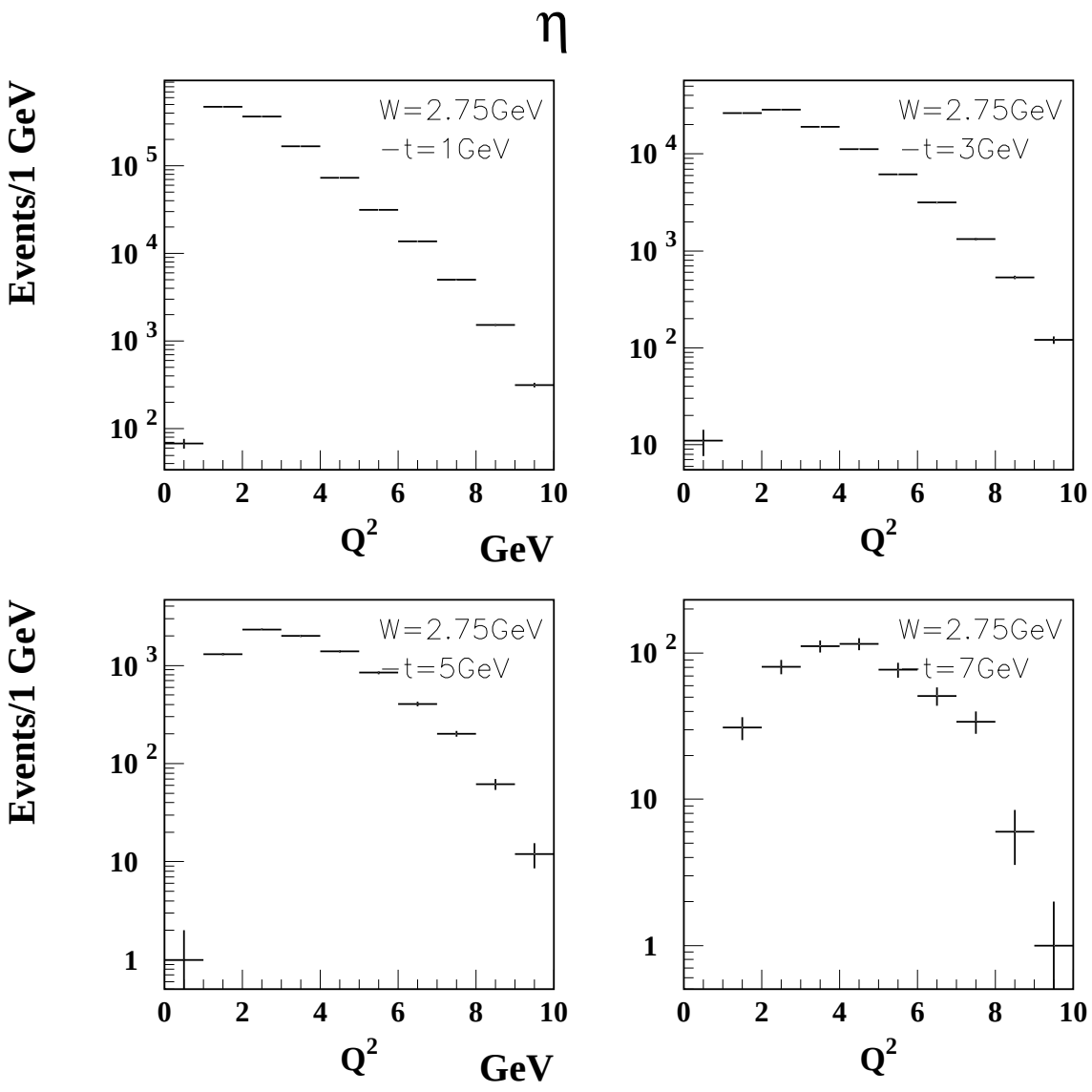

FIG. 39: Reaction $ep \to ep\eta$, $\eta \to \gamma\gamma$. Q^2 distribution for $W = 2.75 \pm 0.75$ and different t bins with $\Delta t = 2$ Gev^2. Statistics corresponds to 1000 hours of the CLAS12 operation.

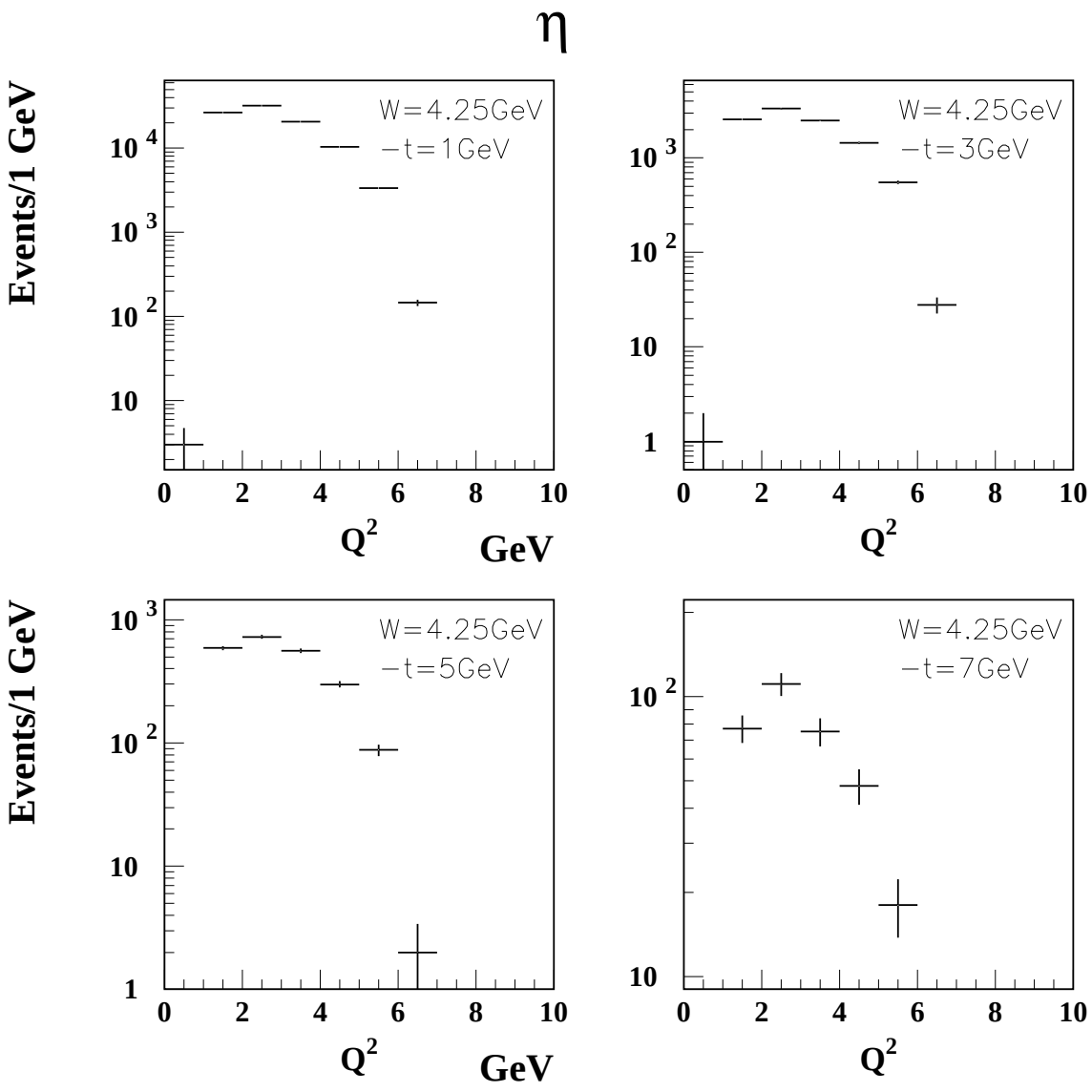

FIG. 40: Reaction $ep \to ep\eta$, $\eta \to \gamma\gamma$. Q^2 distribution for $W = 4.25 \pm 0.75$ and different t bins with $\Delta t = 2$ Gev^2. Statistics corresponds to 1000 hours of the CLAS12 operation.